Available online at www.sciencedirect.com
SCIENCE DIRECT
Remote Sensing of Environment 96 (2005) 375 – 398
Remote Sensing of Environment
www.elsevier.com/locate/rse

Hyperspectral discrimination of tropical rain forest tree species at leaf to crown scales

Matthew L. Clark[a,*], Dar A. Roberts[a], David B. Clark[b]

[a]Department of Geography, University of California, Santa Barbara, Santa Barbra, CA 93106, United States
[b]University of Missouri-St. Louis, St. Louis, MO, USA, and La Selva Biological Station, Puerto Viejo de Sarapiquí, Costa Rica

Received 1 August 2004; received in revised form 24 March 2005; accepted 26 March 2005

Abstract

We investigated the utility of high spectral and spatial resolution imagery for the automated species-level classification of individual tree crowns (ITCs) in a tropical rain forest (TRF). Laboratory spectrometer and airborne reflectance spectra (161 bands, 437–2434 nm) were acquired from seven species of emergent trees. Analyses focused on leaf-, pixel- and crown-scale spectra. We first described the spectral regions and factors that most influence spectral separability among species. Next, spectral-based species classification was performed using linear discriminant analysis (LDA), maximum likelihood (ML) and spectral angle mapper (SAM) classifiers applied to combinations of bands from a stepwise-selection procedure. Optimal regions of the spectrum for species discrimination varied with scale. However, near-infrared (700–1327 nm) bands were consistently important regions across all scales. Bands in the visible region (437–700 nm) and shortwave infrared (1994–2435 nm) were more important at pixel and crown scales. Overall classification accuracy decreased from leaf scales measured in the laboratory to pixel and crown scales measured from the airborne sensor. Leaf-scale classification using LDA and 40 bands had 100% overall accuracy. Pixel-scale spectra from sunlit regions of crowns were classified with 88% overall accuracy using a ML classifier and 60 bands. The highest crown-scale (ITC) accuracy was 92% with LDA and 30 bands. Producer's accuracies ranged from 70% to 100% and User's accuracies ranged from 81% to 100%. The SAM classifier performed poorly at all scales and spectral regions of analysis. ITCs were also classified using an object-based approach in which crown species labels were assigned according to the majority class of classified pixels within a crown. An overall accuracy of 86% was achieved with an object-based LDA classifier applied to 30 bands of data. Object-based and crown-scale ITC classifications were significantly more accurate with 10 narrow-bands relative to accuracies achieved with simulated multispectral, broadband data. We concluded that high spectral and spatial resolution imagery acquired over TRF canopy has substantial potential for automated ITC species discrimination.

Keywords: Tropical rain forest; Individual tree crown classification; Tree floristic classification; Hyperspectral sensors; Multispectral data; High spatial and spectral resolution; Linear discriminant analysis; Spectral angle mapper; Maximum likelihood

1. Introduction

1.1. Importance of tropical rain forest trees

Tropical rain forests (TRF) now cover only 6.4% of the Earth's terrestrial surface yet they maintain a large proportion of the world's biotic diversity (Thomas et al., 2004; Whitmore, 1990). TRF biodiversity is imperiled by wide-spread deforestation, logging and landscape-scale (e.g., 10^1–10^5 ha) forest fragmentation (Achard et al., 2002; Fearnside, 1999). At individual crown to landscape scales, tropical trees have a dominant role in maintaining this rich biota because they define the horizontal and vertical substrate, food resources, and gradients of light, moisture, and temperature. Furthermore, tropical tree biomass also represents a major pool of terrestrial carbon (Clark et al., 2003; Dixon et al., 1994). Warmer global temperatures linked to greenhouse gas emissions may alter tree growth

* Corresponding author. Tel.: +1 805 893 4434; fax: +1 805 893 3146.
E-mail address: mclark@geog.ucsb.edu (M.L. Clark).

0034-4257/$ - see front matter © 2005 Elsevier Inc. All rights reserved.
doi:10.1016/j.rse.2005.03.009

rates, recruitment and mortality, thereby creating new assemblages of trees as global temperatures increase (Clark et al., 2003; Laurance et al., 2004). It is expected that biodiversity will decline if these altered tree communities fail to sustain the complex interactions among trees, pollinators, seed dispersers, herbivores, symbiotic fungi and other species that are common in tropical forests (Laurance et al., 2004). One recent global-scale study concluded that climate-change effects on tropical forests over the next 50 years may pose as much risk to species survival as deforestation (Thomas et al., 2004).

1.2. Contribution of remote sensing to tropical rain forest assessment

Our understanding, monitoring, conservation and management of tropical rain forests is greatly hindered by a lack of spatially- and temporally-extensive information on tree floristic composition, species richness and structure. Mainly due to prohibitive costs and inaccessibility, most available data comes from relatively small field plots with infrequent re-sampling intervals. It is difficult to generalize such field data to the landscape, regional and global scales needed for understanding the important processes affecting biodiversity (Foody et al., 2003; Tuomisto et al., 2003). Passive optical remote sensors provide multi-scale, continuous spatial, and frequent temporal measurements of radiance from TRF canopies that can be linked to species composition and richness of trees and other organisms as well as to forest structure (Foody, 2003; Foody et al., 2003; Gillespie et al., 2004; Nagendra, 2001; Tuomisto et al., 2003). Remote sensing applications in the tropics have relied upon medium spatial resolution imagery from multispectral spaceborne sensors (e.g., Landsat Thematic Mapper with 30-m pixels, 6 optical bands). This imagery is inexpensive and has permitted mapping of general forest cover classes for calculating the rate and extent of regional deforestation and forest fragmentation (Cochrane et al., 1999; Roberts et al., 2002; Skole & Tucker, 1993; Steininger et al., 2001). However, variability in forest types due to high tree diversity and both natural and human disturbances results in complex radiance signals that are difficult to discriminate using coarse spectral and spatial resolution sensors, leading to significant errors in estimates of land cover area and temporal change (Achard et al., 2002; Cochrane et al., 1999; Foody, 2003; Powell et al., 2004; Skole & Tucker, 1993).

A new generation of high spatial resolution (<4 m), multispectral sensors now exists for use by tropical resource managers and scientists that can resolve individual tree crowns (ITCs) as groups of image pixels (Gougeon & Leckie, 2003; McGraw et al., 1998). ITCs can be identified to species and regrouped into communities, stands or patches (Gougeon & Leckie, 2003; Leckie et al., 2003). Such capabilities in the tropics could greatly improve multi-scale forest classifications of tree floristic composition, species richness, habitat, and disturbance history. Furthermore, temporal ITC analyses may provide a means to systematically monitor regional long-term changes in keystone, endemic, rare or commercial tree species due to logging and climatic change (Clark, Read et al., 2004a; Gougeon & Leckie, 2003; Nagendra, 2001; Read et al., 2003; Trichon, 2001).

1.2.1. Individual tree crown (ITC) discrimination in high spatial resolution imagery

Visual interpretation of high spatial resolution aerial photographs from film cameras has been the traditional method in forestry for the species-level identification of ITCs in high-latitude conifer and deciduous hardwood stands of relatively low tree diversity. There are few studies from tropical sites—where tree species richness can be >300 species per hectare (Trichon, 2001; Whitmore, 1990). Previous studies involved the visual interpretation of 1:600 to 1:6000 scale natural-color aerial photographs using various subjective criteria, such as crown hue, shape, texture, foliage density and phenology (Clément & Guellec, 1974; Herwitz et al., 1998; Myers & Benson, 1981; Trichon, 2001). Myers and Benson (1981) found that 22% of canopy tree species in Queensland, Australia could be identified with >75% accuracy and there was considerable variation in accuracy among interpreters.

New digital forms of high spatial resolution imagery from cameras, videography, and multispectral airborne and spaceborne sensors (e.g., IKONOS, Quickbird) have stimulated the development of automated techniques for ITC detection, crown delineation and subsequent measurement of crown architecture and floristic information (reviewed in McGraw et al., 1998 and Nagendra, 2001). Automated ITC delineation and classification algorithms have been optimized for distinguishing trees in northern-latitude forests dominated by conifers and deciduous hardwoods (Gougeon, 1995; Key et al., 2001; Leckie & Gougeon, 1999; Meyer et al., 1996), and it is unclear how these algorithms will perform in TRF with high species diversity and complex canopies.

1.2.2. Hyperspectral discrimination of tropical tree species

Hand-held, airborne and spaceborne hyperspectral optical sensors measure spectral information in over 50 narrow bands spanning the visible (VIS=437–700 nm), near-infrared (NIR=700–1327 nm), and two shortwave-infrared (SWIR1=1467–1771 nm; SWIR2=1994–2435 nm) regions of the electromagnetic spectrum (region ranges adapted from Asner, 1998). It is anticipated that the automated classification of tropical species may be possible with hyperspectral imagery that is both fine enough to resolve ITC objects and also measures pertinent discriminatory spectral features from 400 to 2500 nm (Cochrane, 2000); however, this hypothesis has remained untested with an airborne or spaceborne hyperspectral sensor. In this study, our field spectrometer and high spatial resolution hyperspectral data offer an unprecedented opportunity to

explore the spatial-scale dependency of spectral reflectance in the remote identification of tree species. Below we briefly discuss important factors that influence plant reflectance at various spatial scales and that may affect the automatic discrimination of tree species.

1.2.3. Reflectance properties at leaf, branch and crown scales

Leaf-scale reflectance spectra are controlled by 1) leaf biochemical properties (e.g., water, photosynthetic pigments, structural carbohydrates), which create wavelength-specific absorption features, and 2) leaf morphology (e.g., cell-wall thickness, air spaces, cuticle wax), which affects photon scattering (Asner, 1998, Grant, 1987; Roberts et al., 2004; Woolley, 1971). VIS spectral variability among species is low due to strong absorption by chlorophyll (Cochrane, 2000; Poorter et al., 1995). High NIR transmittance and reflectance result from photon scattering within leaf air-cell wall interfaces, such as in spongy mesophyll (Gausman, 1985; Grant, 1987; Woolley, 1971). In SWIR1 and SWIR2, water absorption tends to obscure other absorption features produced by biochemical constituents (e.g., lignin and cellulose) (Asner, 1998; Gausman, 1985).

Branch-scale spectra, such as from a high resolution pixel (e.g.,<4 m) or measured in situ with a hand-held spectrometer, are a mixture of radiance determined by the proportion, physical arrangement, and reflective and transmittive properties of crown tissues, including leaves, stems, branches, fruits, and flowers. Photon multiple-scattering among these components will tend to increase the expression of leaf biochemical absorption features, especially within crowns with large, densely-distributed and/or horizontally-oriented leaves (Asner, 1998). Fine-scale shadows cast within the branch may depress overall reflectance. Relative to leaf scales, these factors are known to increase branch-scale spectral variability and enhance separability of northern-latitude conifer and broadleaf trees (Roberts et al., 2004). Fung et al. (1998) used laboratory-derived, branch-scale hyperspectral data (400–900 nm, 90 evenly-spaced bands) and a linear discriminant classifier to discriminate 12 subtropical tree species. An overall accuracy of 84% was achieved and individual species Producer's accuracies ranged from 56% to 100%. Species spectral separability was attributed to the effect of leaf-size variation expressed at the branch scale. Gong et al. (1997) found that a neural network classifier applied to sunlit first-derivative spectra (6–8 cm spatial resolution, in situ) could classify 6 conifer species with an average overall accuracy of 91%.

At the crown scale, the three-dimensional architectural arrangement of foliage and non-photosynthetic components determines the amount of photon volumetric-scattering and attenuation within the crown (Asner, 1998). van Aardt and Wynne (2001) have shown that the VIS, NIR and SWIR1 regions are useful for discriminating species of temperate forest conifer and hardwood species when using in situ crown-scale hyperspectral data (sunlit sides of crowns). Spectral derivatives provided the best overall classification accuracies, which were 84% for conifer species and 93% for hardwood species. Cochrane (2000) provides the only investigation of TRF crown-scale hyperspectral data for automated species recognition (350–1050 nm data). The study used laboratory spectra from 11 tree species to simulate branch and crown scales. Target species discrimination was possible at crown scales, while it deteriorated at branch and leaf scales. Crown-scale spectra were best separated in the VIS–NIR transition (i.e., the "red edge") and NIR regions. However, because the analysis used simulated branch and crown-scale spectra, it is not known how non-photosynthetic vegetation or volumetric crown scattering will affect tree species spectral separability.

Tropical rain forests pose challenging obstacles to ITC classification. TRF tree communities are characterized by high diversity and relative rarity of individuals, so large image extents are needed to find representative training samples. Many trees occur below a dense overstory canopy, preventing their detection by a passive optical sensor. In lowland tropical forests, a relatively constant growing season fosters a diversity of phenological traits, and leaf flush and flowering may follow annual or irregular cycles with no overriding community-scale patterns (Newstrom et al., 1994). Therefore, strategically-timed over-flights to capture spectrally-important phenological events (sensu Key et al., 2001) may be done for only a few tree species that have well-characterized phenology. Moreover, leaf-turnover and flower display may be asynchronous among and within individual crowns of the same species, thereby increasing intraspecific variability in leaf- to crown-scale spectra. For example, long-lived leaves within a crown may be covered with epiphylls, which combined with leaf necrosis decrease VIS and increase NIR reflectance (Roberts, Nelson et al., 1998). Depending on the density of leaves in a crown, which may vary in time, radiance from understory shrubs, sub-canopy trees, lianas, bark lichens, canopy soil, and epiphytes may mix with a target species radiance and increase intraspecific spectral variability. It is not yet clear whether these spectral components will increase branch- and crown-scale within-species variation to a level that inhibits among-species spectral discrimination (Castro-Esau et al., 2004; Cochrane, 2000).

1.3. Objectives

In this study, we examine the relative trade-offs between spectral features, spatial scale of measurement, and classification schemes for the automated classification of individual TRF tree species using their reflectance properties. Field spectrometer and airborne hyperspectral reflectance spectra (161 bands, 437–2434 nm) were acquired from seven species of emergent trees in a lowland tropical rain

forest, permitting analyses at leaf, pixel and crown scales. Our main objectives were to:

- Determine if spectral variation among TRF tree species (interspecific) is greater than spectral variation within species (intraspecific), thereby permitting spectral-based species discrimination.
- Identify the spatial scale and spectral regions that provide optimal discrimination among TRF emergent tree species.
- Develop an analytical procedure for the species-level (floristic) classification of individual tree crowns using their reflectance spectra.
- Assess the relative importance of narrowband hyperspectral versus broadband multispectral information for species identification of TRF trees.

2. Methods

2.1. Study site and materials

2.1.1. Study site

This study was conducted at the La Selva Biological Station (LSBS), in the Sarapiquí canton of Costa Rica (84°00′13.0″ W, 10°25′52.5″ N) in areas of old-growth, swamp and secondary forests within the extent bounded by the hyperspectral imagery (Fig. 1). Precipitation averages 4244 mm annually, with a comparatively dry season from January to April and a second smaller dry season from August to October (Frankie et al., 1974; Organization for Tropical Studies [OTS] meteorological data 1957–2003, http://www.ots.ac.cr). The old-growth forest (Fig. 2A) is classified as a Tropical Wet Forest in the Holdridge Life Zone System and is characterized by a species-rich, multilayered community of trees, palms, lianas, and other terrestrial and epiphytic plants (Hartshorn & Hammel, 1994). There are at least 400 species of hardwood trees. Although some overstory trees can be completely deciduous for a part of the year, mainly in the dry season, the canopy is considered evergreen (Frankie et al., 1974; Hartshorn & Hammel, 1994).

2.1.2. Canopy-emergent trees

To select our study species, we conducted field surveys and took advantage of a Geographic Information System (GIS) database of tree locations from a long-term tree demography study at LSBS (the TREES project; Clark et al., 1998). Our preliminary analysis involved 544 individual trees belonging to 27 species and led us to focus our efforts on seven species (Table 1) of canopy emergents for which there were sufficient individuals in the hyperspectral imagery (Section 2.1.4) for a representative sample. Emergent trees with large, exposed crowns provided a large sample of pixels that were less influenced by spectral shadowing or scattering by neighboring trees, and they were easy to locate in the orthorectified hyperspectral imagery (e.g., Fig. 2A and B). Furthermore, five of the seven study species (BAEL, DIPA, HYME, HYAL and LEAM) are under analysis in the TREES project, providing opportunities to generalize local-scale research (e.g., demographic changes) to broader spatial scales using remote sensing.

A total of 214 individuals of the seven study species were identified in the hyperspectral imagery through field surveys conducted between January 2000 and July 2001 (Table 2). The trunk coordinates in the LSBS grid system (see Clark, Clark et al., 2004b) were surveyed by

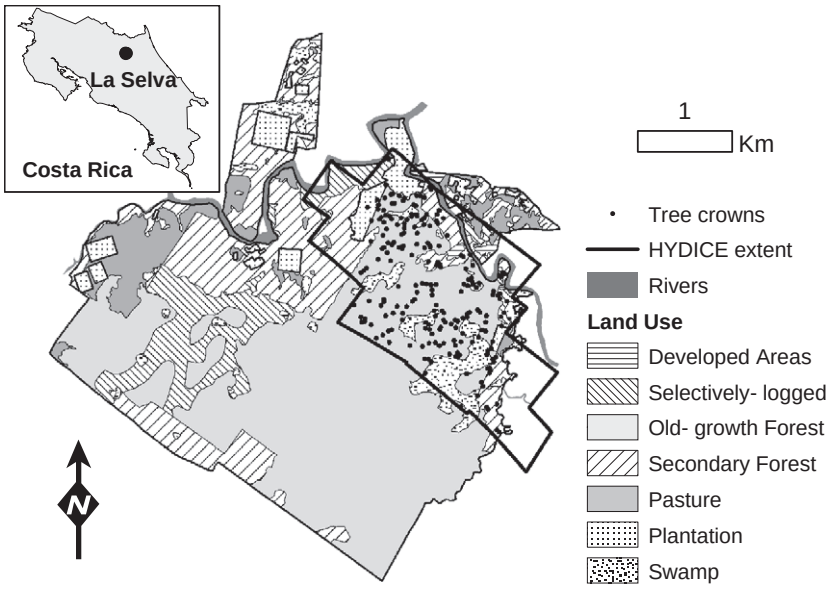

Fig. 1. The La Selva Biological Station study site and extent of HYDICE hyperspectral imagery. The 214 study crowns are labeled with points.

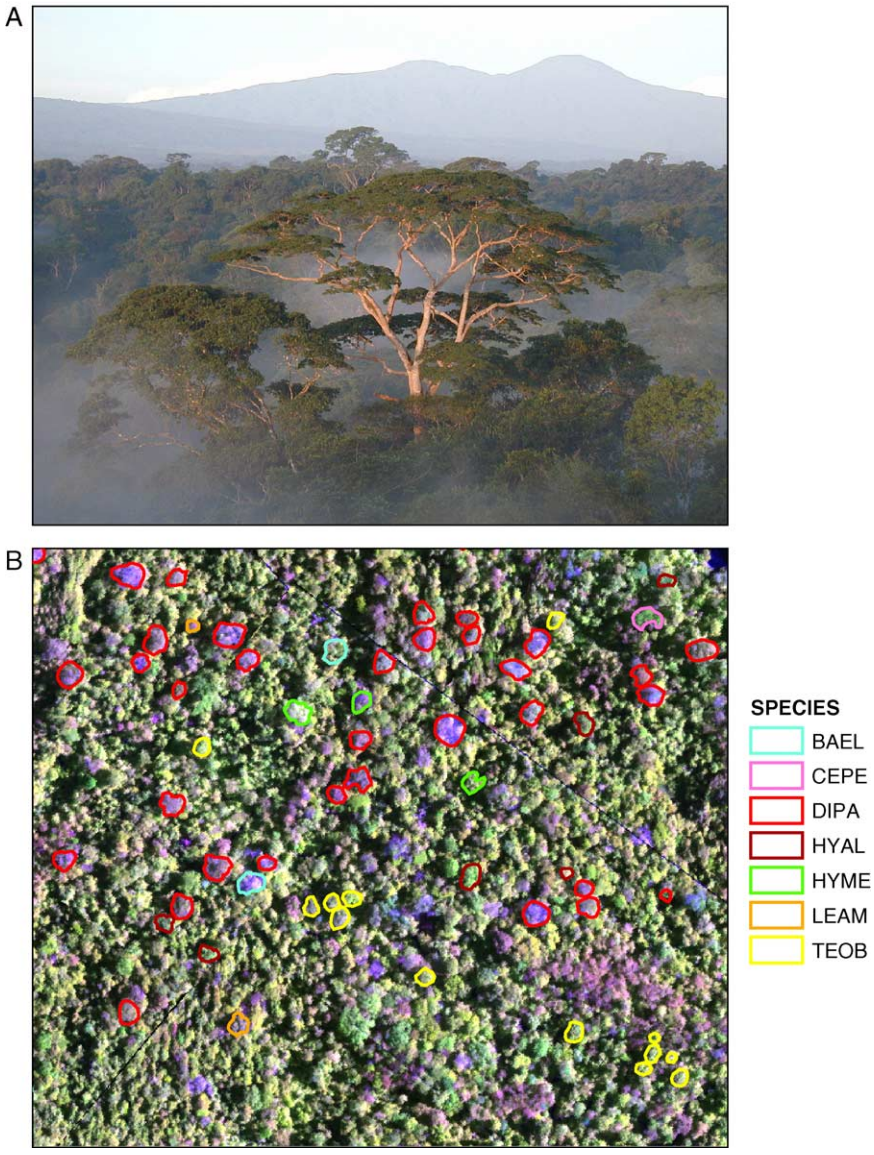

Fig. 2. (A) View of old-growth Tropical Wet Forest at the La Selva Biological Station. The canopy-emergent tree in the foreground is *Balizia elegans*. (B) Example of 1.6-m spatial resolution HYDICE hyperspectral imagery over old-growth canopy (Red: 1651 nm [SWIR2], Green: 835 nm [NIR], Blue: 661 nm [Red]) with overlaid individual tree crown polygons. Map scale is 1:3000.

measuring the distance and angle of the trunk from the nearest grid tube. These trunk coordinates were then converted from LSBS grid coordinates to the UTM projection, WGS-84 datum coordinate system using a least-squares affine transformation with RMSE of 4.8 m (OTS, unpublished data).

Table 1
Study tree species attributes (Adapted from Frankie et al., 1974, O'Brien, 2001 and personal observation)

Tree species [family or sub-family]	Code	Leaf phenology functional group	Leaf exchange timing	March 30 leaf cover[a]
Balizia elegans(Ducke) Barneby and Grimes [Mimosoideae]	BAEL	Deciduous	Annual	High
Ceiba pentandra Gaertn. [Bombacaceae]	CEPE	Deciduous	Annual	High
Dipteryx panamensis (Pittier) Record and Mell [Papilionoideae]	DIPA	Deciduous	Annual	Low
Hyeronima alchorneoides Allemão [Euphorbiaceae]	HYAL	Evergreen	Continuous	High
Hymenolobium mesoamericanum Lima [Papilionoideae]	HYME	Deciduous	Sub-annual	High
Lecythis ampla Miers [Lecythidaceae]	LEAM	Deciduous	Annual	Low
Terminalia oblonga (Ruiz and Pav.) Steud. [Combretaceae]	TEOB	Evergreen	Continuous	High

[a] Leaf cover is for late-March to early-April, and is what would be expected for the majority of individuals for each species based on available literature data and personal field observations.

Table 2
Summary of characteristics of individual tree crowns from HYDICE data

Tree species	No. of crowns	Crown area, m^2 mean (range)	All pixels/crown mean (range)	Sunlit pixels/crown mean (range)
BAEL	29	358 (108–699)	140 (42–273)	68 (19–131)
CEPE	10	766 (361–1695)	299 (141–662)	153 (62–338)
DIPA	81	519 (141–1167)	203 (55–456)	98 (28–227)
HYAL	34	388 (159–635)	152 (62–248)	78 (34–118)
HYME	14	479 (108–1009)	187 (42–394)	99 (23–185)
LEAM	21	349 (164–630)	136 (64–246)	67 (31–136)
TEOB	25	312 (105–543)	122 (41–212)	64 (21–110)
All	214	444 (105–1695)	174 (41–662)	87 (19–338)

Species names defined in Table 1.

There is little long-term data on leaf and flowering phenology of the study species. Some overstory tree species are deciduous and completely drop and flush leaves, generally beginning in the first dry season, while others are evergreen and continuously flush small amounts of leaves throughout the year (Table 1). Hyperspectral imagery was acquired on March 30, 1998 (Section 2.1.4), at the end of the first dry season, and all study trees were expected to have high mature leaf cover (i.e., high leaf area index) except DIPA and LEAM (personal observation, April 12, 2004; literature data [Frankie et al., 1974; O'Brien, 2001]; summarized in Table 1). Although we do not have field observations from our study individuals during the image acquisition, O'Brien (2001) estimated leaf cover of BAEL, DIPA, HYME and LEAM individuals at LSBS that were 30–60 cm diameter above buttress and unobstructed or emergent crowns. Data included March through April, 1998 and showed that a relatively large proportion of DIPA and LEAM individuals had low mature leaf cover, while BAEL and HYME individuals had higher mature leaf cover.

2.1.3. Leaf-scale spectra

A shotgun was used to shoot 152 leaf samples down from crowns of individual study trees in August, 2002 (Table 3). Three to five individual trees from each of the seven study species were selected for sampling, and 2–10 leaves per individual were shot down from the upper, sun-exposed part of the crown. Leaf samples included a range of maturity and health. Individual leaflets >1 cm width were sampled from separate leaves for species with compound leaves (CEPE, DIPA, HYME) and leaflets were analyzed as leaves. For scale considerations discussed below, BAEL compound leaves were analyzed rather than individual leaflets. Bidirectional reflectance properties of the "leaves" (i.e., leaves or leaflets) were measured in a darkroom at LSBS. Leaf samples were put in a plastic bag with a moist paper towel and stored in a cooler with ice until refrigerated in the laboratory. All samples were measured within 12 h of collection. A single 150-W halogen lamp was placed with a 25° incident angle and 53 cm above a matte-black, 5% reflective box. An ASD FieldSpec spectrometer (Analytical Spectral Devices, Boulder, CO, USA) sensor with an 8° fore-optic was positioned 7.1 cm at nadir above the box center, yielding a 1-cm sensor field of view (FOV). The spectrometer was optimized with a white Spectralon® panel (Labsphere, North Sutton, NH, USA) placed in the box center, and the instrument was re-optimized using the panel after measuring every 5–7 leaf samples. Leaf samples were placed in the box center with adaxial (upper) surfaces to the sensor and radiance was measured 5 times per leaf. Bidirectional reflectance of a single leaf sample will vary across its surface depending on biochemical variation (e.g., chlorophyll concentration, leaf necrosis, epiphyll cover), structural properties (e.g., cuticle texture, mesophyll depth), and illumination and sensor geometry. To capture this potential spectral variation from an individual leaf, leaf orientation and position relative to the sensor FOV were varied with each of the 5 radiance measurements (i.e., the leaf was moved while the sensor remained stationary). Radiance spectra from the Spectralon® panel were used as a standard to convert leaf radiance to percent reflectance. The final leaf reflectance spectrum was an average of the five reflectance spectra from each leaf.

Individual leaflets of BAEL (*Balizia*) leaves were smaller than the sensor FOV, thus causing the black background to mix with the radiance signal. To counteract this effect, each *Balizia* leaf was stacked on top of 3 other *Balizia* leaves to simulate a dense layer of leaves. The leaf-stack position and orientation was haphazardly varied with each radiance measurement.

2.1.4. Hyperspectral imagery

The U.S. Naval Research Laboratory flew the airborne HYperspectral Digital Imagery Collection Experiment (HYDICE) sensor over LSBS in March 30, 1998, which corresponds to the end of the drier season in the region. HYDICE is a push-broom, indium-antimonide hyperspectral sensor that measures 210 bands covering the 400–2500 nm region of the electromagnetic spectrum (Basedow et al., 1995). The La Selva flights were flown at a 3.17–3.20-km altitude between 7:55–8:27 a.m. local time (13:55–14:27 UTC). Six runs of 0.5-km wide, variable length, 1.6-m spatial resolution data (0.5 mrad instantaneous field of view; IFOV) were acquired over old-growth forest, secondary forest, selectively-logged forest, tree plantations, pastures and the nearby town of La Guaria. HYDICE runs were

Table 3
Laboratory leaf spectra summary

Tree species	No. of samples	No. trees sampled (leaves per tree)
BAEL	16	3 (5–6)
CEPE	15	3 (5)
DIPA	30	5 (3–10)
HYAL	23	4 (6–10)
HYME	30	3 (6–10)
LEAM	14	3 (2–6)
TEOB	24	4 (5–7)
All	152	25

Species names defined in Table 1.

delivered as 16-bit calibrated radiance data. Individual tree crowns are clearly resolved in this high spatial and spectral resolution imagery (Fig. 2B). The morning data acquisition avoided afternoon cloud cover yet the 56.3° to 48.4° solar zenith angles (92° to 94° azimuth angles) during the flight caused deep tree shadows that are particularly noticeable in old-growth forest canopy gaps (Fig. 2B).

We orthorectified the LSBS sections of HYDICE runs 6, 9, 12 and 15 using the Erdas IMAGINE OrthoBASE software package (Leica Geosystems GIS and Mapping, LCC, Atlanta, GA, USA). Runs were segmented into 800-m long blocks and each block was orthorectified with 21–75 ground control points collected by visually matching emergent tree crown centers in HYDICE imagery to co-located crown centers in a 0.3-m lidar digital canopy model (DCM; Clark et al., 2004b). Terrain distortions in the imagery were corrected in the orthorectification processing with a 10-m resolution digital terrain model (DTM: OTS, unpublished data), which was originally derived from Laser Vegetation Imaging Sensor (LVIS) lidar data (Rocchio, 2000). Orthorectification used a nearest-neighbor interpolator and geo-registered the HYDICE imagery in the Universal Transverse Mercator (UTM), WGS-84 datum projection of the DCM and DTM reference data (Fig. 1 shows spatial extent of runs).

The ACORN v4.0 (Analytical Imaging and Geophysics LLC, Boulder, Colorado) atmospheric correction package was used for calibrating radiance values to surface reflectance. Although atmospheric water vapor can be calculated on a per pixel basis (Gao & Goetz, 1990), low signal-to-noise in principal water absorption bands for HYDICE (Basedow et al., 1995) produced considerable spatial error in water vapor estimates; and therefore, atmospheric corrections were performed with a fixed precipitable water vapor of 32 mm. A tropical atmospheric model was used with atmospheric visibility of 100 km. Water vapor and visibility parameters were established based on visual assessment of old-growth tree spectra and an empirical, minimum root-mean square error (RMSE) comparison with field-collected spectra. Field spectra were measured in August, 2002 with an ASD FieldSpec spectrometer and included gravel road, cement, tile, exposed soil, wood planks, green metal roof-tops, and mowed lawn targets that were located within the HYDICE runs. An 8° fore-optic was positioned about 1.5 m above a target and sensor radiance was converted to reflectance using an in situ white Spectralon® calibration panel. Five individual reflectance measurements were averaged to create a target spectrum over a 1 m^2 area, and then several of these spectra were collected over a homogenous area of the target and then averaged.

Wavelength calibration differed among runs by 0.61–2.67 nm per wavelength (HYDICE metadata, U.S. Naval Research Laboratory). Atmospheric correction was performed using each run's respective band centers and full-width half-maximum (FWHM) parameters. A common set of band center wavelengths were calculated by averaging bands centers from the four runs, and reflectance values from each run were then linearly-interpolated to this common set of center wavelengths. Band centers were spaced an average distance of 6 nm in VIS, 14 nm in NIR, 12 nm in the SWIR1 and 9 nm in SWIR2. Post-calibration reflectance artifacts (e.g., spikes near water absorption features) were minimized with a 3-channel boxcar filter. Bands with extreme noise in spectral regions less than 437 nm and greater than 2435 nm, as well as bands in the strong water absorption features 1313–1466 nm and 1771–1994 nm, were removed from analyses.

An example comparison between final HYDICE reflectance and field-measured ASD reflectance for a wooden-plank suspension bridge and a nearby tree crown (*Pentaclethra macrophylla*) is shown in Fig. 3. The HYDICE reflectance spectra were generally the same shape, but reflectance was much lower than field spectrometer measurements in the SWIR1 and SWIR2 regions. This pattern was observed in comparing HYDICE with other field spectra. NIR reflectance peaks were high and water absorption features centered at 980 and 1200 nm were deep relative to field spectra, especially for the wooden bridge. These artifacts in HYDICE derive from a combination of poor radiometric calibration, sensor noise, atmospheric noise (e.g., water vapor absorption) and the difference in time between HYDICE and field measurements. Field measurements were taken on August 2, 2002 (9:30 a.m.) while HYDICE was acquired on March 30, 1998 (8 a.m.). If atmospheric conditions were constant over the reserve, all HYDICE artifacts should be common to all HYDICE spectra because the same parameters were used to convert each pixel to reflectance. The mismatch between HYDICE reflectance and expected reflectance affects our analysis in three ways: 1) in comparing HYDICE spectra to laboratory leaf spectra, 2) possibly shifting band selection towards bands with higher signal to noise, and 3) limiting the comparison of our results with other sensors.

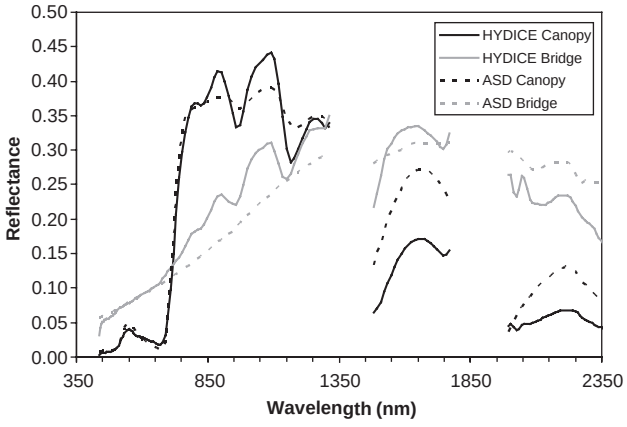

Fig. 3. Reflectance spectra from airborne HYDICE and field ASD spectrometers for a wooden bridge (over dark water) and a *Pentaclethra macrophylla* crown. The *Pentaclethra* ASD spectrum was acquired from the bridge.

2.1.5. Simulated broadband, multispectral imagery

HYDICE reflectance spectra were convolved using sensor-specific spectral response functions to simulate IKONOS, Landsat ETM+, and ASTER (Advanced Spaceborne Thermal Emission and Reflection Radiometer) imagery. Although each of these sensors has a different spatial resolution (i.e., 4 m IKONOS, 30 m ETM+, 15–30 m ASTER), the spatial resolution of simulated imagery was fixed at the 1.6 m of HYDICE imagery. Also, by using simulated imagery, the same artifacts evident in HYDICE (Section 2.1.4) were incorporated into simulated spectra. Therefore using simulated multispectral imagery reduced the effects of spatial scale and radiometric artifacts on inter-sensor comparisons.

2.1.6. Pixel- and crown-scale spectra from individual tree crowns

Field-surveyed trunk locations were overlaid on the orthorectified HYDICE mosaic and the polygons representing the 2-dimensional area of the tree crowns were manually digitized over the imagery. We used the DCM (Section 2.1.4) as a visual aid to determine a crown's shape in areas with shaded pixels. The average crown area for the study species was 444 m^2, with each crown comprising from 41–662 pixels (Table 2). Hereafter we refer to the digitized crown polygons as individual tree crowns (ITCs: Gougeon & Leckie, 2003).

Our analyses differentiated between all ($Pixel_{ALL}$) and sunlit-only ($Pixel_{SUN}$) pixels within each ITC. Sunlit pixel spectra were designated as all pixels within an ITC that had reflectance greater than or equal to the crown's mean 800-nm (NIR) reflectance (Gougeon, 1995). Crown-scale spectra were calculated by averaging either all ($Crown_{ALL}$) or sunlit-only ($Crown_{SUN}$) pixel spectra within each ITC.

2.2. Data analysis

2.2.1. Testing of within and among species spectral variability

Spectral separability of species should be optimal if different species have high statistical distance in feature space and within-species variation is less than among-species variation. We tested the null hypothesis that within- and among-species spectral variation are equal with a non-parametric multivariate analysis of variance technique (NPMANOVA) first developed for use with ecological distance matrices (Anderson, 2001; McArdle & Anderson, 2001). In remote sensing applications, the spectral angle is a metric used for comparing the degree of similarity between two spectra (Kruse et al., 1993). Unlike Euclidean distance, the spectral angle is insensitive to linearly-scaled differences among spectra such as those caused by illumination. In our implementation of the NPMANOVA, the distance between each spectrum to every other within- and among-species spectrum was computed using the spectral angle and Euclidean distance, and distances were stored in $N \times N$ distance matrices (N=number of observations). In the calculation of spectral distance, spectra were analyzed using the entire 161-bands or limited to the VIS, NIR, SWIR1, SWIR2 regions. A pseudo-F statistic was calculated as the ratio of among to within species sums of squares (Anderson, 2001; McArdle & Anderson, 2001). The null hypothesis tested was that within and among species spectral variation was equal, which would make the F-ratio close to one. The significance of the F-ratio was tested against a null distribution of F created by 5000 random permutations of the distance matrix (Anderson, 2001). For pixel-scale NPMANOVA tests, 200 pixels for each species were randomly selected from crowns for the respective species. For leaf- and crown-scale NPMANOVA tests, we used all available spectra due to limited sample sizes. We performed NPMANOVA tests using the DISTLM2 v.5 software program (Anderson, 2004).

2.2.2. Species classification schemes

We explored three popular supervised classification schemes for TRF tree classification: spectral angle mapper (SAM), linear discriminant analysis (LDA), and the maximum likelihood (ML) classifier. SAM is a spectral matching technique (Kruse et al., 1993). The spectral angles (Section 2.2.1) between each sample spectrum and several reference spectra are computed to reduce the hyperspectral data cube from an n-dimensional spectral space to a similarity space with dimensions equal to the number of reference spectra (i.e., classes). In this study, SAM classification was accomplished by assigning each sample spectrum to the class with the closest similarity (i.e., lowest spectral angle), and no maximum-angle threshold was used to minimize false detections. LDA is a common classifier that has been used in previous ITC classification research (Fung et al., 1998; Gong et al., 1997; van Aardt & Wynne, 2001). For LDA classification, the pooled within-class covariance matrix and predictor variables (e.g., reflectance values) from training samples are used to build classification equations, or discriminant functions for each class (Duda & Hart, 1973; Tabachnick & Fidell, 1989). A class is chosen based on the highest a posteriori probability calculated from the functions. The most important assumption of LDA classification is that all classes share the same covariance matrix (i.e., homogeneity). In the ML classifier, each class mean, standard deviation and covariance matrix are estimated from the training data to evaluate a sample's class a posteriori membership probability (Duda & Hart, 1973). ML has been widely used in ITC species classification (Gougeon, 1995; Key et al., 2001; Leckie et al., 2003; Meyer et al., 1996).

Supervised classification schemes are often stymied by the large dimensionality of hyperspectral imagery. Fine resolution spectral bands are often correlated and so represent redundant information. Also, sensor noise such as stripes from bad detectors or atmospheric attenuation may be greater in certain bands and this noise may increase class variance and decrease class separability. With the ML

classifier in particular, it has been shown that the within-class covariance matrix can be poorly estimated when there are few training samples relative to the data dimensionality, leading to a decrease in classifier performance called the Hughes phenomenon (Duda & Hart, 1973; Jackson & Landgrebe, 2001). Hence, the use of ML is limited for hyperspectral remote sensing of forested areas because image dimensionality is high while training data are expensive or difficult to acquire. A common solution to this dilemma is to reduce data dimensionality through spectral feature (i.e., band) selection. In this study, we used a forward stepwise selection method based on discriminant analysis (Tabachnick & Fidell, 1989; van Aardt & Wynne, 2001). This method was implemented using the SAS STEPDISC procedure (SAS Institute Inc., Cary, NC, USA) with the significance criteria set at $\alpha = 0.05$ for all analyses except the crown scale, which had criteria set to $\alpha = 0.20$.

Following feature selection, SAM, LDA and ML classifiers were applied to leaf-, pixel- and crown-scale spectra to assess how the spatial scale of spectral measurements affects species classification accuracy. At each scale, the *n*-dimensional spectral space was varied to include the full-spectra dataset (161 bands), spectral regions (i.e., VIS, NIR), or LDA stepwise-selected bands. Spectral regions were sub-sampled to include only 10 bands per region. These bands were evenly-spaced with an average spacing of 23 nm (VIS), 55 nm (NIR), 25 nm (SWIR1), and 47 nm (SWIR2). The same set of classifiers was also applied to the simulated broadband multispectral data (Section 2.1.5). All LDA classification was accomplished using the "MASS" package in the R statistical environment (R Development Core Team, 2004; MASS 7.2–12, R v2.0) while SAM and ML classification was performed in ENVI v4.1 and IDL v6.1 (RSI, Inc., Boulder, CO, USA).

2.2.3. Crown-scale and "object-based" ITC classification

A major objective of this study was to assess optical remote sensing for operational, ITC species discrimination. Current research shows that tree species discrimination is best accomplished by aggregating pixels into their respective crowns for object-based (as opposed to pixel-based) classification using spectral and spatial properties (Gougeon, 1995; Leckie et al., 2003; Meyer et al., 1996). In this study, the species of ITCs in the HYDICE imagery were determined by 1) the class assigned from crown-scale spectra, $\text{Crown}_{\text{ALL}}$ or $\text{Crown}_{\text{SUN}}$ and, 2) taking the majority value of the classified pixels ($\text{Pixel}_{\text{ALL}}$ or $\text{Pixel}_{\text{SUN}}$) within each ITC, i.e., the "winner-takes-all" rule (Meyer et al., 1996). We refer to this latter approach (2) as "object-based" ITC classification.

2.2.4. Classifier training and accuracy assessment

For pixel-scale classifications, 300 randomly-selected training pixels were sampled from the crown objects for each species (300 pixels × 7 species = 2100 training pixels). Pixels were sampled from the whole crown ($\text{Pixel}_{\text{ALL}}$) or from sunlit regions of the crown ($\text{Pixel}_{\text{SUN}}$), and each crown was sampled unless it had fewer than 40 pixels. Each classifier (LDA, ML or SAM) was applied to the remaining non-training pixels within each crown. We sampled 300 training pixels per species to provide a robust estimation of ML class covariance statistics. For pixel-scale testing, 300 non-training classified pixels per species were randomly selected (300 pixels × 7 species = 2100 test pixels). A new set of 300 test pixels was randomly selected for each classifier-band combination analyzed.

For crown-scale and object-based analyses, classification training and testing were performed with cross-validation due to the limited number of ITCs (Duda & Hart, 1973; Krzanowski, 2001). We sequentially left one ITC out and trained classifiers with pixel- or crown-scale spectra from the remaining 213 ITCs (i.e., "leave-one-out" cross validation). For object-based classification, each withheld crown was classified based on the majority-class rule (Section 2.2.3). Cross validation provides a slightly biased estimate of true classifier accuracy (Krzanowski, 2001). Statistical differences among classifications were tested with the *Z* statistic computed from the Kappa statistic and variance (Congalton & Mead, 1983; Hudson & Ramm, 1987). Leaf-scale classification was also performed with a similar cross-validation procedure.

3. Results

3.1. Reflectance properties at different scales

3.1.1. Leaf-scale spectra

Leaf-scale spectra for the seven tree species (Fig. 4) showed typical patterns of vegetation: low VIS reflectance caused by absorption by chlorophyll and other pigments, high NIR reflectance due to multiple-scattering within the leaf structure, weak NIR water absorption features at 980 and 1200 nm, and moderate reflectance in SWIR1 and SWIR2 with peaks at 1650 and 2200 nm caused by dominant water absorption features at 1400, 1900 and 2700 nm (Gausman, 1985; Roberts et al., 2004).

There was considerable variation in reflectance within species, especially in the NIR and SWIR (Fig. 4). Several factors can cause leaf spectral variation within a given species, including epiphyll cover, herbivory, necrosis, maturation of the mesophyll, and the concentration of chlorophyll and water. Seven percent of all upper-canopy leaves sampled had epiphyll coverage. As seen for HYME leaves of roughly the same age (Fig. 5A), epiphyll coverage tends to lower the green peak and NIR reflectance, possibly due to more absorption of light by epiphylls covering the adaxial leaf surface. Herbivory is another factor that affected 4% of the leaves sampled. For LEAM leaves of the same age, some leaves had light

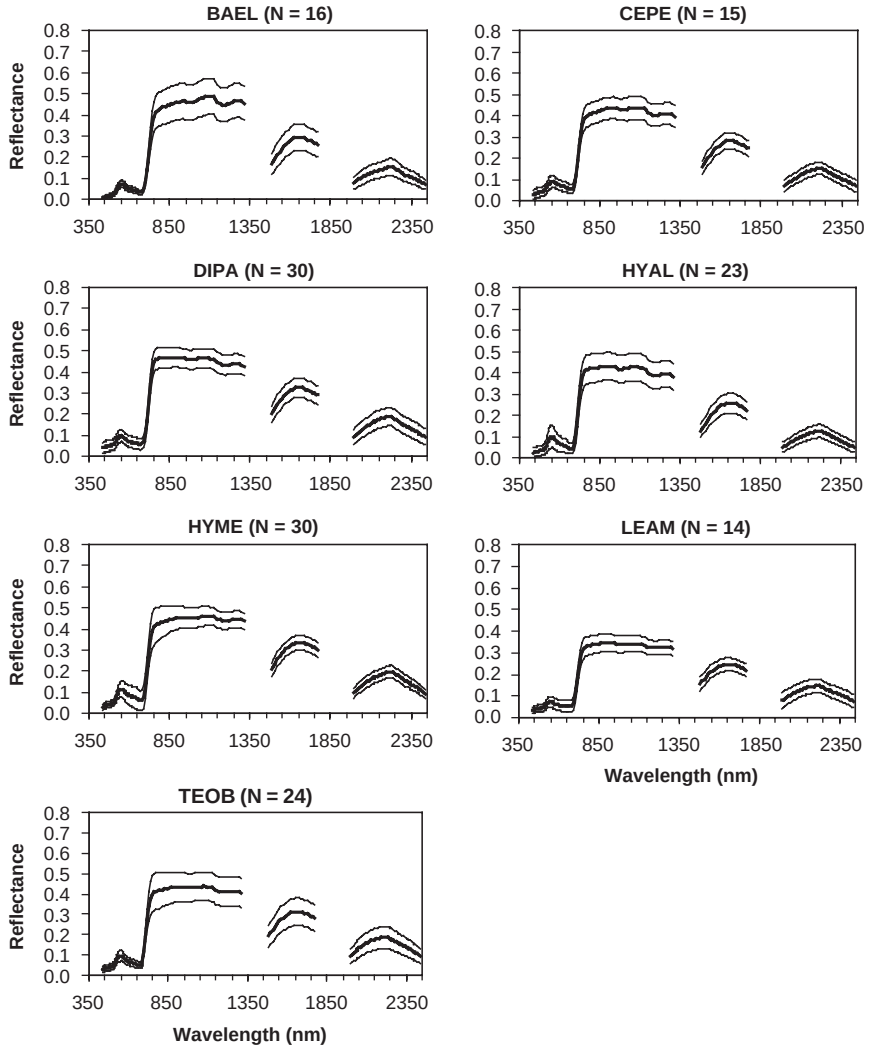

Fig. 4. Leaf scale mean (bold line) and standard deviation (±1 S.D., thin line) of reflectance by species. Species codes are listed in Table 1.

brown-colored leaf mines caused by an insect. As the percentage of these mines increased, there was less VIS absorption (higher reflectance) likely due to lower amounts of photosynthetic pigments from eaten leaf material, and increased NIR and SWIR reflectance (Fig. 5B) likely due to lower water content and more exposed non-photosynthetic leaf material (e.g., residual, dried leaf veins). Finally, leaf age is an important factor because it determines time exposed to epiphylls and herbivory, as well as internal leaf architecture and chemical properties. For TEOB, young thin leaves had high red and low NIR, SWIR1 and SWIR2 reflectance relative to mature, thicker leaves (Fig. 5C). Thin leaves are compact and have fewer air-cell wall refractive discontinuities than mature leaves, causing lower NIR–SWIR reflectance (Gausman, 1985). Also, lower chlorophyll content in young leaves likely accounts for higher VIS reflectance (i.e., lower VIS absorption) in the blue (450 nm) and red (680 nm) regions (Gausman, 1985; Woolley, 1971). As the leaf senesces, lower concentrations of chlorophyll greatly reduce the amount of absorption throughout the VIS, thereby increasing reflectance (Fig. 5C).

3.1.2. Pixel-scale spectra

Pixel-scale spectra revealed the same general patterns of NIR scattering and chlorophyll and water absorption as seen in leaf-scale spectra (Fig. 6). Relative to leaf-scale spectra, there was an overall reduction (darkening) of percent reflectance in $Pixel_{ALL}$ and $Pixel_{SUN}$ spectra (Table 4). Darkening of spectra is partly due to fine-scale shadows within branches of leaves and other crown materials, especially in the $Pixel_{ALL}$ samples. However, as noted in Section 2.1.4, some of the darkening in the SWIR1 and SWIR2 regions of pixel spectra was due to poor HYDICE radiometric calibration. Roberts et al. (2004) found that biochemical absorption properties of leaves were accentuated at the pixel scale by the multiple-scattering of photons among leaves and other crown tissues within the hyperspectral sensor's FOV. Our spectra show evidence of this phenomenon; photon scattering can

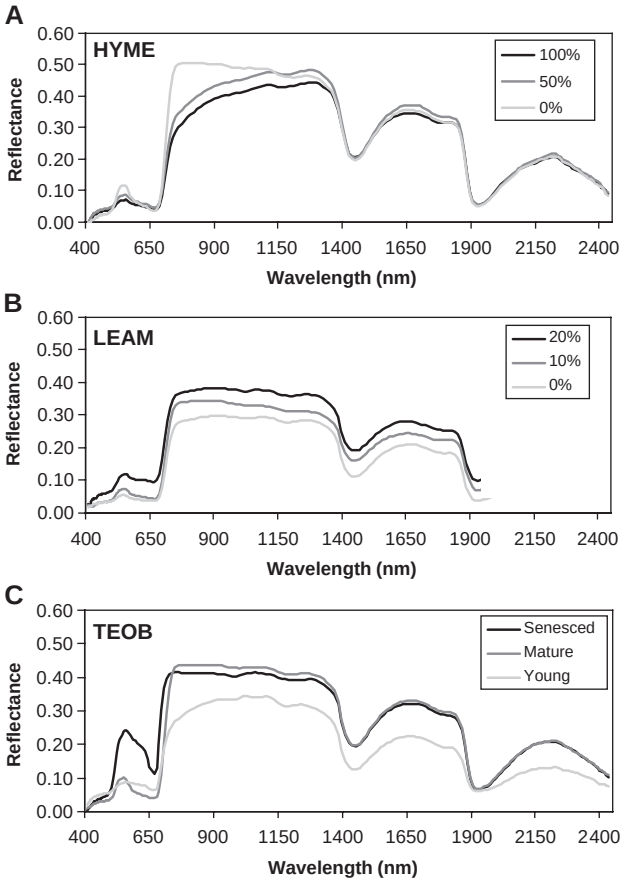

Fig. 5. Leaf-scale variation in spectral properties. (A) *Hymenolobium mesoamericanum* leaves: percent area covered by a single species of epiphyll. (B) *Lecythis ampla* leaves: percent area of leaf herbivory (i.e., light brown-colored mines) caused by a leaf-mining insect. (C) *Terminalia oblonga* leaves: leaf aging from young to senesced leaves. Note: All spectra in Fig. 5 were from upper-canopy leaves and were included in leaf-scale spectral analyses except for the *Terminalia* senesced leaf, which was collected on the ground.

partially explain why NIR water absorption features at 980 and 1200 nm were deeper in pixels relative to leaf-scale samples (Fig. 6).

The arrangement and density of crown tissues will govern the crown scattering environment and the degree to which leaf biochemical properties are accentuated at pixel or crown scales (discussed in Section 1.2.3). Considering sunlit pixels ($Pixel_{SUN}$), DIPA and LEAM had 40.2% and 37.9% NIR reflectance, respectively, while the other species had between 43.8% (CEPE) and 51.5% (TEOB) mean reflectance (Fig. 6). Relatively low NIR reflectance makes DIPA and LEAM appear purple in the image (Fig. 2B, RGB 1651 : 835 : 661 nm). Individuals of these deciduous species had low crown foliage density (i.e., leaf area index, LAI) during HYDICE image acquisition in the late dry season. With fewer leaves in the crown, there was less photon scattering and subsequently, NIR reflectance was low relative to leaf-on species. The variation in scattering environments among species with different crown LAI, explains why the NIR standard deviation was much higher in pixel scales than in leaf scales (Table 4).

3.1.3. Crown-scale spectra

Crown-scale spectra were an average of pixel spectra. The averaging of spectra decreased $Crown_{ALL}$ and $Crown_{SUN}$ variance in all spectral regions relative to $Pixel_{ALL}$ and $Pixel_{SUN}$ variance, respectively (Table 4, Fig. 7). As observed with pixel scales, the mixture of pixels from bright and dark, shadowed parts of the crown tended to lower average reflectance for $Crown_{ALL}$ spectra relative to $Crown_{SUN}$ spectra.

3.2. Among- and within-species spectral distances

Using spectral angle as a distance metric, among-species (interspecific) spectral variability was significantly greater ($p \leq 0.001$) than within-species (intraspecific) variability for all spectral regions at leaf and pixel scales (Table 5). However, species differences at the crown scale were mainly focused in the NIR region. Using Euclidean distance, which includes variation due to illumination, among-species variability was significantly greater ($p \leq 0.001$) than within-species variability at all scales and all spectral regions. The greater separation of species with Euclidean distance over spectral angle distance at crown scales indicates that crown-level illumination differences among species, possibly due to varying crown LAI, tend to increase species separability. There was no advantage to using just sunlit pixels at crown scales ($Crown_{ALL}$ vs. $Crown_{SUN}$). However, at pixel scales sunlit samples had greater separability (i.e., higher *F*-ratios) than when considering all samples. The NIR, SWIR1 and SWIR2 regions of sunlit pixels had particularly high *F*-ratios.

3.3. Selected spectral features

3.3.1. Leaf scale

For discriminating species, 90% of the 10 most important wavelengths selected by the stepwise procedure were concentrated in the NIR and SWIR1 regions (Fig. 8A; Fig. 9A), where there was relatively large variation in percent reflectance (Table 4). *Balizia* leaves had the highest NIR variability (6.7% s.d. for BAEL, 3.3–5.5% s.d. for other species). BAEL variability is likely caused by measuring their reflectance from leaf stacks. Photons have more opportunity for scattering within stacks of leaves, thereby increasing the NIR plateau, broadening water absorption features, and increasing overall NIR variability. SWIR2 had lower variability than NIR or SWIR1 yet SWIR2 comprised 25% of the bands selected when considering 20 bands (Fig. 9B). The VIS had the lowest spectral variability, and only 10% of the bands selected were from VIS when considering 10 or 20 bands. The selected VIS bands were in the blue absorption

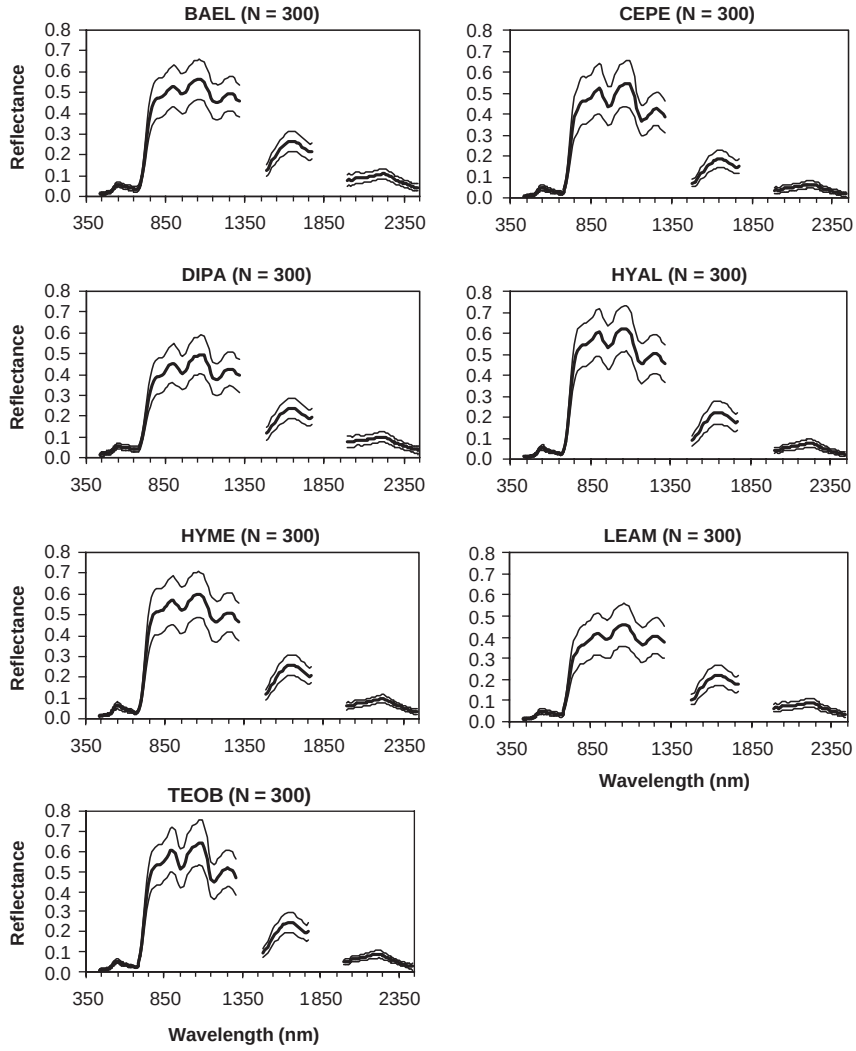

Fig. 6. Mean (bold line) and standard deviation (±1 S.D., thin line) of reflectance by species for sunlit pixels. Species codes are listed in Table 1.

feature at 449 nm, the green peak at 568 nm, and the red-edge at 719 nm (Fig. 8A).

3.3.2. Pixel scale

Leaf-scale band selection is best compared to the $Pixel_{SUN}$ samples because they have a similar range of illumination. Of the 20 most important bands, there were 4 more NIR and 4 fewer SWIR1 bands selected for $Pixel_{SUN}$ relative to leaf-scale spectra (Fig. 8A–B). In terms of the percentage of bands selected (Fig. 9A and B) and NPMANOVA *F*-ratios (Table 5), the NIR region was particularly useful in pixel-scale species discrimination, especially with sunlit samples. Selected NIR bands were concentrated in the red-edge and the plateaus surrounding the water absorption features at 980 and 1200 nm (Fig. 8B), while less so at leaf scales (Fig. 8A). There was high NIR variability relative to other regions (Table 4), which is likely caused by species differences in crown LAI (Section 3.1.2). Low-LAI deciduous species (e.g., DIPA, LEAM) have lower NIR reflectance relative to high-LAI species (e.g., HYAL, TEOB). These differences in crown architecture among species thus create distinctive variation in maximum NIR reflectance that permits clearer NIR species discrimination with pixel spectra relative to leaf spectra, which are not influenced by crown architecture. SWIR1 may be less useful at pixel scales relative to leaf scales due to a combination of greater water absorption and lower sensor signal to noise.

Table 4
Mean and standard deviation (s.d.) of percent reflectance across spectral regions

	VIS	NIR	SWIR1	SWIR2	Full Spectra
Leaf	5.8 (2.8)	41.3 (6.8)	26.3 (5.5)	12.7 (4.2)	20.9 (4.7)
$Pixel_{ALL}$	2.7 (1.4)	34.8 (13.5)	15.1 (6.3)	5.5 (2.6)	14.4 (5.9)
$Pixel_{SUN}$	3.4 (1.1)	44.4 (10.3)	20.2 (4.8)	7.5 (2.3)	18.4 (4.6)
$Crown_{ALL}$	2.7 (0.8)	35.6 (6.9)	15.2 (2.9)	5.8 (1.7)	14.6 (3.0)
$Crown_{SUN}$	3.5 (0.8)	45.0 (7.9)	19.7 (3.1)	6.9 (1.7)	18.5 (3.4)

Mean and s.d. were computed on a band-by-band basis and then averaged for each spectral region.

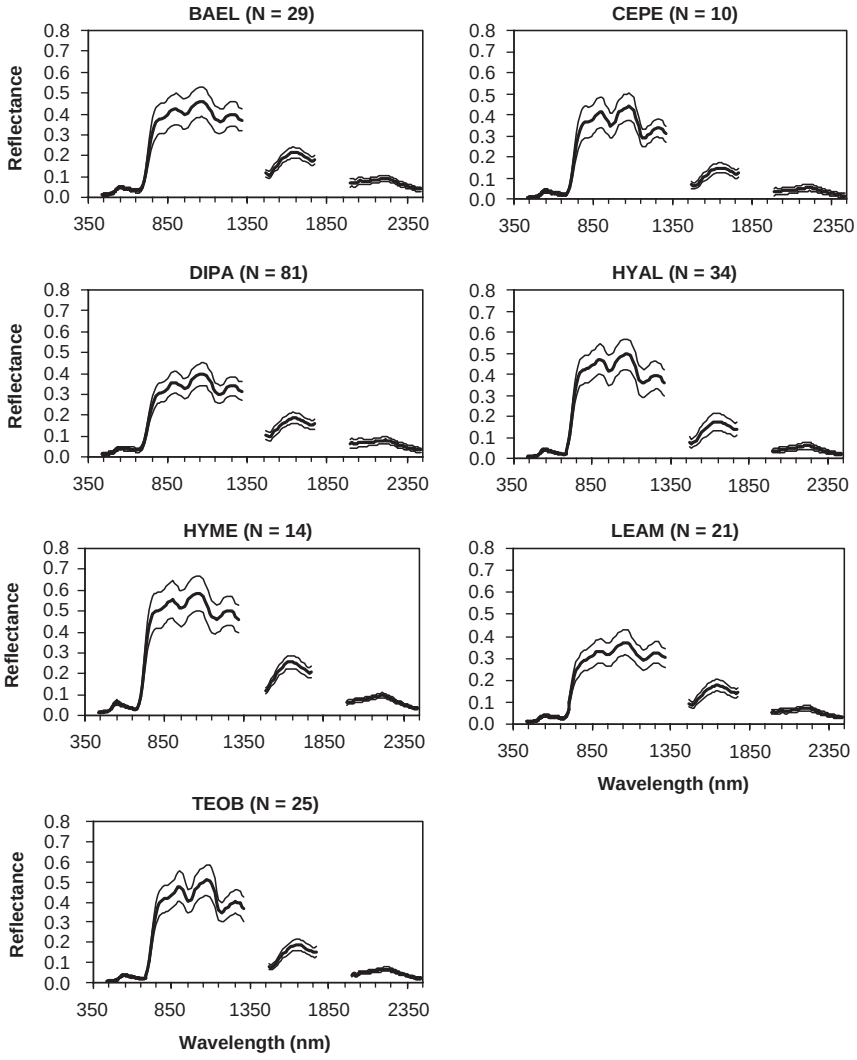

Fig. 7. Crown-scale mean (bold line) and standard deviation (±1 S.D., thin line) of reflectance by species for $Crown_{ALL}$ spectra. Species codes are listed in Table 1.

When considering the best 20 discriminatory bands, NIR was less important when all sunlit and shaded pixels were analyzed, likely due to less photon scattering in shaded pixels (Fig. 8B, 9B). With $Pixel_{ALL}$ samples, there were a similar number of bands in the VIS, NIR and SWIR1 regions. VIS bands were spread across blue-green edge (491 nm), yellow edge (575 and 619 nm) and red well (670 nm) features, while SWIR1 bands were evenly spaced across the region.

3.3.3. Crown scale

With the stepwise band selection procedure, only 42 and 41 bands were significant at the $\alpha = 0.05$ level for $Crown_{ALL}$ and $Crown_{SUN}$ spectra, respectively. The significance criteria was substantially relaxed to $\alpha = 0.2$ in order to select 60 bands for comparison with leaf and pixel scales. The twenty most important bands (all at $\alpha = 0.05$) were concentrated in the VIS, NIR and SWIR2 regions for $Crown_{ALL}$ spectra (Figs. 8C, 9B). For $Crown_{SUN}$ spectra, there were 2 fewer bands in VIS and 2 more bands in SWIR2 relative to $Crown_{ALL}$ spectra. As with the pixel scale, NIR bands were clustered in the red edge and on the peaks bordering the water absorption features.

3.4. Classification of tree species at leaf, pixel and crown scales

3.4.1. Hyperspectral, narrowband classification

The overall accuracies of tree species classifications with different narrowband combinations and classification schemes are presented in Table 6. Leaf-scale maximum likelihood (ML) analysis was limited to 10 bands due to the low number of training samples per class (discussed in Section 2.2.2, Table 3). Linear discriminant analysis (LDA) had the highest accuracy (89.5%) for leaves when the analysis was isolated to the 10 best bands, while ML with 10 bands was 8.6% less accurate ($Z = 6.66$, $p \leq 0.05$). *Balizia* was the only species that had no inter-class confusion with

Table 5
Non-parametric multivariate analysis of variance (NPMANOVA), comparing among- and within-species spectral variation using spectral angle and Euclidean distance

Spectral region	Bands	Leaf scale[a]	Pixel scale	Crown scale
Spectral angle distance				
Full spectra	161	n/a	119.7***	5.4*
Full spectra (sunlit)	161	16.1***	162.3***	7.7***
VIS	43	n/a	68.3***	1.3 ns
VIS (sunlit)	43	13.4***	103.3***	2.5 ns
NIR	46	n/a	113.0***	6.0***
NIR (sunlit)	46	12.6***	137.2***	8.3***
SWIR1	25	n/a	94.2***	0.8 ns
SWIR1 (sunlit)	25	26.6***	128.1***	1.4 ns
SWIR2	48	n/a	32.3***	3.0 ns
SWIR2 (sunlit)	48	10.2***	78.3***	3.6*
Euclidean distance				
Full spectra	161	n/a	28.6***	3.7***
Full spectra (sunlit)	161	13.4***	180.3***	3.7***
VIS	43	n/a	13.1***	4.6***
VIS (sunlit)	43	4.1***	51.2***	4.5***
NIR	46	n/a	34.1***	2.8***
NIR (sunlit)	46	12.8***	195.7***	2.6***
SWIR1	25	n/a	16.4***	4.4***
SWIR1 (sunlit)	25	18.4***	133.7***	4.4***
SWIR2	48	n/a	61.2***	3.8***
SWIR2 (sunlit)	48	18.6***	157.4***	3.8***

Values are F ratios. In all analyses, 5000 permutations were used to test significance. Significance is: ns=not significant, $*p \leq 0.05$, $**p \leq 0.01$, $***p \leq 0.001$.
[a] Artificial illumination from halogen lamp.

the LDA classifier and 10+ bands nor with LDA with NIR or SWIR1 bands, which can be attributed to its distinct spectral leaf-stack properties (Section 3.3.1). LDA accuracy was significantly higher with 20 bands ($Z=3.15$; $p \leq 0.05$) and overall accuracy reached 100% with 40 bands (no significant difference between 20 and 30–60 bands).

Both band selection and NPMANOVA identified the SWIR1 region as important to species separability at leaf scales, while the VIS region was not as important (Fig. 9, Table 5). In agreement with these findings, 10 SWIR1 bands provided the highest classification accuracy of the spectral regions while 10 VIS bands produced relatively low accuracy (Table 6, LDA or ML). Relative to LDA and ML classifiers, the Spectral Angle Mapper (SAM) classifier had relatively poor performance (<51% overall accuracy) and differences among band combinations will not be discussed.

At the pixel scale, ML generally had higher overall accuracy than LDA for most band combinations, using all or sunlit-only pixels (Table 6). SAM had very low performance, with no accuracy exceeding 50%. In the ML and LDA analyses, $Pixel_{SUN}$ classifications were significantly more accurate than when using $Pixel_{ALL}$ samples (Table 6, arrows). Best pixel-scale performance was with 40–60 bands from $Pixel_{SUN}$ samples with either classifier (differences not significant). ML classification with 161 bands (full-spectra) was significantly lower than when using 20–60 bands due to the Hughes phenomenon (Section 2.2.2), while full spectra information did not dramatically change LDA accuracy. Classification accuracies for both LDA and ML were significantly higher with 10 bands from across the entire spectra relative to selecting 10 bands from specific spectral regions.

The LDA classifier applied to crown-scale spectra produced some of the highest species classification accuracies using airborne HYDICE imagery. For all band combinations, LDA accuracies were not significantly greater with $Crown_{ALL}$ versus $Crown_{SUN}$ samples. LDA classification accuracy using 10 optimally-selected bands was significantly greater than using all 161 bands or 10 evenly-spaced bands in the VIS, NIR, SWIR1 and SWIR2 spectral regions.

The best accuracy was 92.1% when the LDA classifier was applied to 30 $Crown_{ALL}$ stepwise-selected bands (Tables 6 and 7). However, 20 bands provided only 2.8% less overall accuracy and were not significantly different than 30 bands. Of the 30 bands used in the $Crown_{ALL}$

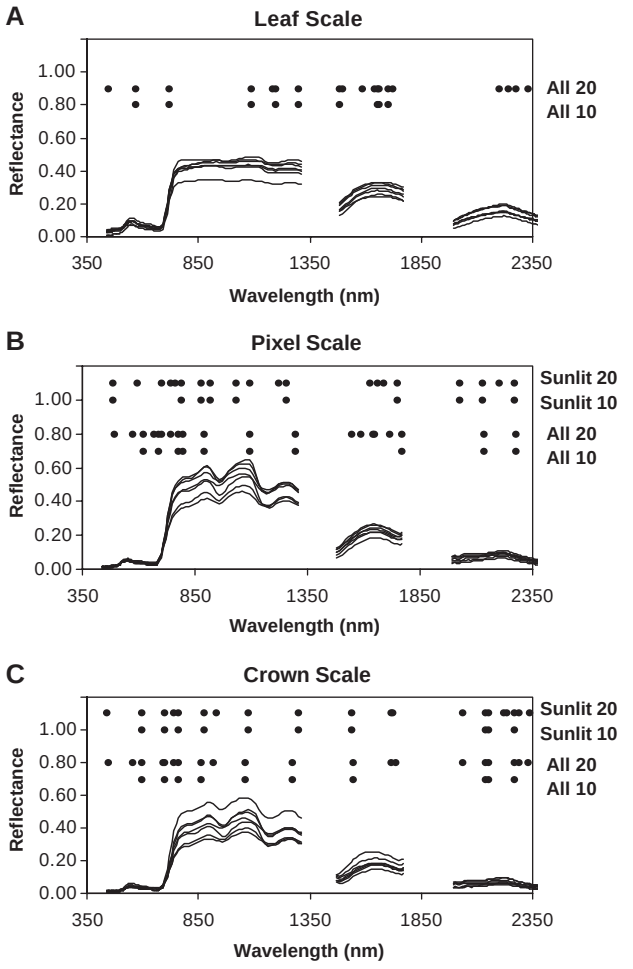

Fig. 8. Mean reflectance spectra for the seven study species at (A) leaf, (B) pixel and (C) crown scales from Figs. 4, 6 and 7, respectively. Pixel and crown spectra were computed from sunlit-only (Sun) and all (All) pixel spectra prior to band selection. $Pixel_{SUN}$ and $Crown_{ALL}$ spectra are displayed in (B) and (C), respectively. Dots above spectra represent the best 10 and 20 bands selected by the stepwise-selection procedure.

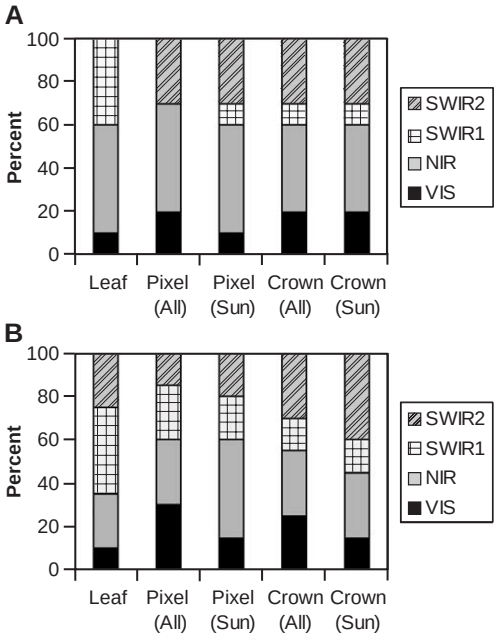

Fig. 9. The percentage of 10 (A) and 20 (B) stepwise-selected bands within each spectral region at leaf, pixel and crown scales.

classification, 30.0% were within the NIR region while 23.3% were in each of the other 3 spectral regions. Forty-one percent of misclassified ITCs involved confusion between DIPA and LEAM. This result was expected because both species had similar reflectance properties due to low-LAI crowns.

Although it was not possible to compare LDA and ML classifiers for data dimensionalities >10 bands due to limited training data, the cross-validation accuracies between LDA and ML with 10-bands were significantly higher for LDA–7.5% and 7.0% higher with $Crown_{ALL}$ or $Crown_{SUN}$, respectively. As with other scales of analysis, SAM crown-scale classification accuracy was relatively low. The highest SAM accuracy achieved was only 53.7%.

In all LDA and ML classification analyses, there were no minimum a posteriori probability criteria set for assigning samples to a class; and therefore, there were no unclassified samples. The criteria was omitted to permit a direct comparison of LDA and ML with the SAM classifier. For crown-scale LDA classifications, we also experimented with 50%, 75% and 90% probability thresholds, where a crown-scale spectrum (i.e., ITC) was classified as "unknown" if its maximum class a posteriori probability was lower than the specified threshold. As the probability threshold was increased (i.e., made more conservative), more ITCs were labeled as unclassified and the overall accuracy dropped (Fig. 10). The decrease in overall accuracy was less severe as more bands were added to the analysis. With 30 bands, overall classification accuracy was 8.9% significantly higher with no probability threshold relative to a 90% threshold (Tables 7 and 8). A higher probability threshold acted to increase omission errors by switching correctly-classified ITCs to "unknown", thereby decreasing the class Producer's accuracies. In this example, 19 correctly-classified ITCs did not meet the threshold criteria and so were left unclassified. On the other hand, a more conservative threshold decreased commission errors, thereby increasing class User's accuracies. For example, the 90% threshold identified 3 ITCs that had been confused between DIPA and

Table 6
Overall accuracy of classifiers using leaf-, pixel- and crown-scale narrowband (HYDICE) spectra

Bands[a]	Leaf[b]	Pixel[c]			Crown[b]			Object-based[b]		
	All	All		Sunlit	All		Sunlit	All		Sunlit
Linear Discriminant Analysis (LDA)										
10[a]	89.5	67.5	→	72.1	84.1	ns	84.6	74.8	ns	81.8
20[a]	98.0	75.0	→	81.7	89.3	ns	85.5	81.3	ns	83.2
30[a]	99.3	79.0	→	83.2	92.1	ns	87.9	83.6	ns	85.5
40[a]	100.0	79.2	→	86.5	90.2	ns	89.7	84.1	ns	84.1
50[a]	100.0	79.7	→	85.2	89.7	ns	91.1	83.6	ns	85.5
60[a]	100.0	80.6	→	85.4	89.7	ns	90.2	84.1	ns	84.1
161 (Full)	88.8	80.9	→	85.5	61.2	ns	67.8	81.8	ns	83.6
VIS[d]	60.5	45.1	→	53.1	65.9	ns	66.4	62.1	ns	67.3
NIR[d]	80.9	54.7	→	61.5	67.8	ns	67.3	60.3	ns	66.4
SWIR1[d]	88.8	55.1	→	59.8	69.2	ns	68.7	64.0	ns	71.5
SWIR2[d]	81.6	47.8	→	57.6	75.7	ns	76.6	64.5	ns	69.6
Maximum Likelihood (ML)										
10[a]	80.9	69.5	→	76.1	76.6	ns	77.6	77.6	ns	79.4
20[a]	n/a	76.4	→	86.2		n/a		84.6	ns	82.7
30[a]	n/a	79.5	→	86.7		n/a		82.7	ns	80.4
40[a]	n/a	81.6	→	86.9		n/a		82.2	ns	80.4
50[a]	n/a	81.2	→	87.3		n/a		79.0	ns	79.9
60[a]	n/a	79.9	→	87.6		n/a		78.0	ns	77.6
161 (Full)	n/a	68.3	→	79.1		n/a		71.0	ns	71.5
VIS[d]	64.5	49.7	→	58.7	30.4	ns	27.1	62.6	ns	67.3
NIR[d]	71.7	59.6	→	66.3	50.0	←	37.9	69.2	ns	70.1
SWIR1[d]	82.2	53.5	→	66.2	34.1	→	46.7	66.8	ns	69.2
SWIR2[d]	71.1	49.2	→	58.1	39.7	ns	49.1	65.4	ns	71.0
Spectral Angle Mapper (SAM)										
10[a]	46.1	42.4	ns	44.1	45.8	ns	50.9	48.6	ns	42.5
20[a]	50.7	37.9	→	48.9	46.3	ns	53.7	48.1	ns	56.5
30[a]	48.0	39.8	→	48.6	46.7	ns	47.7	46.3	ns	50.9
40[a]	48.7	39.2	→	46.4	45.8	ns	50.5	46.3	ns	52.8
50[a]	47.4	38.9	→	47.0	46.7	ns	51.4	47.7	ns	53.3
60[a]	46.1	38.0	→	48.4	46.3	ns	50.5	46.3	ns	50.0
161 (Full)	48.7	38.7	→	48.4	44.4	ns	48.6	43.9	ns	47.2
VIS[d]	35.5	38.8	→	42.1	14.0	ns	12.6	41.6	ns	43.0
NIR[d]	38.2	42.3	→	47.1	37.4	ns	39.3	48.6	ns	49.5
SWIR1[d]	37.5	33.5	→	38.0	45.3	ns	51.9	37.4	ns	41.6
SWIR2[d]	36.8	31.6	→	36.8	45.8	ns	44.9	43.0	ns	39.3

Leaf-scale data were simulated HYDICE spectra from laboratory measurements. "Object-based" refers to ITC classification using a class-majority rule applied to classified within-crown pixels. Arrows represent the direction of significant improvement in overall accuracy between using all and sunlit-only samples (ns = not significant at $\alpha = 0.05$).

[a] Bands selected using a Linear Discriminant Analysis (LDA) forward, stepwise selection procedure. Significance criteria $\alpha = 0.05$ for leaf, pixel and crown objects, $\alpha = 0.2$ for $Crown_{ALL}$ and $Crown_{SUN}$ spectra.

[b] Accuracy results are from cross validation of samples.

[c] Training and testing data were two mutually-exclusive sets of 300 randomly-selected pixels per species.

[d] VIS, NIR, SWIR1 and SWIR2 regions have 10 evenly-spaced bands (see Section 2.2.2).

Table 7
Error matrix for crown-scale classification using 30 bands and a Linear Discriminant Analysis classifier with no a posteriori probability threshold (Kappa=0.90)

Species	Field reference								
	BAEL	CEPE	DIPA	HYAL	HYME	LEAM	TEOB	Total	User
Classification									
BAEL	27	–	1	–	–	–	–	28	96.4%
CEPE	–	7	1	–	–	–	–	8	87.5%
DIPA	1	2	75	1	1	4	–	84	89.3%
HYAL	1	–	–	33	–	–	–	34	97.1%
HYME	–	–	1	–	13	–	–	14	92.9%
LEAM	–	1	3	–	–	17	–	21	81.0%
TEOB	–	–	–	–	–	–	25	25	100.0%
Unknown	–	–	–	–	–	–	–	–	
Total	29	10	81	34	14	21	25	214	96.4%
Producer	93.1%	70.0%	92.6%	97.1%	92.9%	81.0%	100.0%		92.1%

Species names defined in Table 1.

LEAM due to low a posteriori probabilities. With the threshold set, these crowns were left unclassified and User's accuracy increased 2.5% and 11.3% for DIPA and LEAM, respectively (Tables 7 and 8).

In our classification analyses, only 7 of over 300 tree species were classified. In an operational classification, a probability threshold or other technique will be necessary to ensure that ITCs that are not target species remain unclassified. We tested the crown scale, threshold classifier against non-target ITCs. A total of 30 emergent crowns comprising 14 non-target species were identified in the field and digitized over the imagery, following methods used for the 7 study species. We then classified these non-target ITCs with the 30-band, LDA classifier and a 90% a posteriori probability threshold. The classifier was only trained with the 7 study species (214 ITCs). Five of the non-target ITCs were actually classified as "unknown," whereas 17 were classified as HYAL, 6 as DIPA, 1 as BAEL and 1 as CEPE. Misclassifications were not random. Crowns that were misclassified as DIPA had very similar spectral properties as true DIPA crowns—appearing as purple ITCs in false-color imagery (e.g., Fig. 2B)—suggesting that they had low-LAI crowns. In contrast, ITCs misclassified as HYAL had spectral properties of the high-LAI crowns typical of true HYAL crowns. Our classifier thus appears most attuned to differentiating ITC phenology and structure rather than clear species distinctions.

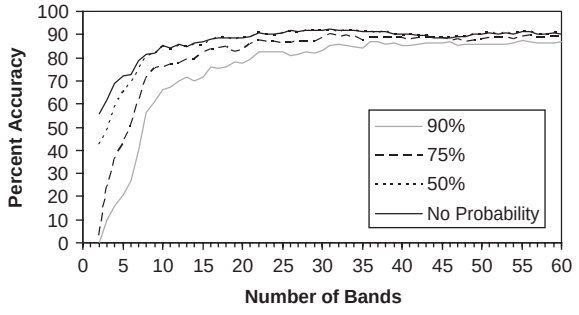

Fig. 10. Crown-scale classification overall accuracy with the addition of bands. Bands were added based on their ranking using a stepwise procedure and the classifier was linear discriminant analysis (LDA). The a posteriori LDA probability required for a crown to be classified was adjusted to four different thresholds: no probability threshold, 50%, 75% and 90% thresholds.

3.4.2. Multispectral, broadband classification

Classification accuracies from simulated broadband sensors (Table 9) followed the same general patterns across scales as discussed for narrowband data: LDA and ML classifiers outperformed SAM; there was an increase in accuracy with more bands; and, LDA and ML accuracies were generally higher at crown scales relative to pixel scales. As with narrowband analyses, the LDA classifier was particularly strong at the crown scale. For $Crown_{ALL}$ ASTER spectra (9 bands), overall accuracy was 76.2%, which was 7.9% and 14.0% lower (both significant) than the accuracies achieved with 10 and 30 narrow bands, respectively (Table 6). With $Crown_{ALL}$ LDA analyses, there was a non-significant 7% increase in overall accuracies with 6 ETM+ bands over 4 IKONOS bands, while there were 9.8% and 16.8% significant increases with 9 ASTER bands over IKONOS and ETM+ bands, respectively.

3.5. Object-based classification using within-crown pixels

3.5.1. Hyperspectral, narrowband classification

ITCs were next assigned a species label based on the majority class of pixel scale, narrowband spectra within each crown object (Table 6, object-based). Object-based ITC classification accuracy was not significantly different using $Pixel_{ALL}$ or $Pixel_{SUN}$ within-crown spectra. The best overall object-based accuracies with each classifier-band combination were generally higher than those achieved with comparable pixel-scale classifications, except for LDA with sunlit pixels and 40, 60 or 161 bands (Table 6). The highest object-based accuracy, 85.5%, was achieved with a LDA classifier applied to 30 bands selected from $Pixel_{SUN}$ spectra (Table 10), although accuracy was not significantly less with 10 and 20 band combinations, nor with $Pixel_{ALL}$ spectra.

Table 8
Error matrix for crown-scale classification using 30 bands and a Linear Discriminant Analysis classifier with a 90% a posteriori probability threshold (Kappa=0.79)

Species	Field reference								
	BAEL	CEPE	DIPA	HYAL	HYME	LEAM	TEOB	Total	User
Classification									
BAEL	25	–	1	–	–	–	–	26	96.2%
CEPE	–	6	1	–	–	–	–	7	85.7%
DIPA	1	1	67	–	1	3	–	73	91.8%
HYAL	1	–	–	32	–	–	–	33	97.0%
HYME	–	–	1	–	11	–	–	12	91.7%
LEAM	–	–	1	–	–	12	–	13	92.3%
TEOB	–	–	–	–	–	–	25	25	100.0%
Unknown	2	3	10	2	2	6	–	25	
Total	29	10	81	34	14	21	25	214	
Producer	86.2%	60.0%	82.7%	94.1%	78.6%	57.1%	100.0%		83.2%

Species names defined in Table 1.

For the 30-band LDA classification ($Pixel_{SUN}$), we assessed the percentage of within-crown classified pixels that had the same species label as their corresponding ITC. If a within-crown pixel and its corresponding ITC species labels were the same, the pixel was considered "correctly classified". If pixels were randomly classified, then each crown would likely have only 14% (1 out of 7) of its pixels correctly classified, and ITCs would be assigned to the class that had a pixel majority by chance. We found that the mean percentage of correctly-classified pixels within correctly-labeled ITCs was 89.9% (range 40.0–100.0%). Therefore, although there were misclassified pixels within ITCs, we are confident that crowns were not assigned a correct label by chance. For mislabeled ITCs, the mean of correctly-classified pixels within each crown was 13.7% (range 0.0–47.8%) This indicates that there was substantial spectral variation among individual crowns of a single species—some crowns had very poor pixel classification accuracy, while others had very high accuracy. For example, TEOB crowns were all correctly labeled and individual crowns had an average 91.6% accuracy. In contrast, only 57% of LEAM crowns were correctly-labeled, and correct crowns only averaged 78.9% pixel accuracy. As expected, mislabeled LEAM crowns were mainly dominated by DIPA pixels, the other low-LAI species.

As recommended by Meyer et al. (1996), we next set a 35% pixel-majority threshold for determining the class of an ITC; that is, a crown was labeled unclassified if the majority class comprised less than 35% of within-crown pixels. With the threshold set and a LDA classifier applied to 30 $Pixel_{SUN}$ bands, only 2 ITCs were affected. One ITC was a HYME that had been misclassified as a BAEL, while the

Table 9
Classification results for simulated broadband spectra

Bands[a]	Leaf[b]	Pixel[c]			Crown[b]			Object-based[b]		
	All	All		Sunlit	All		Sunlit	All		Sunlit
Linear Discriminant Analysis (LDA)										
IKONOS[a]	44.7	42.7	→	49.2	59.3	ns	61.7	52.3	ns	59.3
ETM+[d]	57.9	48.6	→	55.8	66.4	ns	66.4	60.3	ns	64.5
ASTER[e]	80.3	56.4	→	64.7	76.2	ns	77.1	66.8	ns	72.0
Maximum Likelihood (ML)										
IKONOS[a]	61.2	45.3	→	55.1	50.5	ns	50.9	48.1	ns	51.9
ETM+[d]	73.7	54.0	→	62.4	62.6	ns	62.1	62.6	ns	65.9
ASTER[e]	83.6	59.4	→	70.4	72.9	ns	72.4	77.6	ns	78.0
Spectral Angle Mapper (SAM)										
IKONOS[a]	40.1	45.3	←	33.6	20.1	ns	31.3	20.1	ns	31.8
ETM+[d]	34.2	32.5	→	35.9	38.3	ns	39.7	34.1	ns	41.1
ASTER[e]	40.1	30.6	→	36.1	41.1	←	31.3	38.3	ns	37.9

Bands are for IKONOS, Landsat ETM+ and ASTER sensors. Scales follow Table 6.
[a] 4 bands—483, 551, 663, 794 nm.
[b] Accuracy results are from cross validation of samples.
[c] Training and testing data were two mutually-exclusive sets of 300 randomly-selected pixels per species.
[d] 6 bands—479, 561, 661, 835, 1651, 2209 nm.
[e] 9 bands—555, 658, 805, 1655, 2166, 2207, 2264, 2333, 2394 nm.

Table 10
Error matrix for object-based classification using 30 bands, sunlit pixels, a Linear Discriminant Analysis classifier, and no pixel-majority threshold

Species	Field reference								
	BAEL	CEPE	DIPA	HYAL	HYME	LEAM	TEOB	Total	User
Classification									
BAEL	24	–	3	3	1	1	–	32	75.0%
CEPE	–	5	–	–	–	–	–	5	100.0%
DIPA	2	5	76	1	1	8	–	93	81.7%
HYAL	2	–	1	30	–	–	–	33	90.9%
HYME	–	–	–	–	11	–	–	11	100.0%
LEAM	–	–	1	–	–	12	–	13	92.3%
TEOB	–	–	–	–	–	–	25	25	100.0%
Unknown	1	–	–	–	1	–	–	2	0.0%
Total	29	10	81	34	14	21	25	214	
Producer	82.8%	50.0%	93.8%	88.2%	78.6%	57.1%	100.0%		85.5%

Species names defined in Table 1.
(Kappa=0.82).

other ITC was a BAEL that had been misclassified as a DIPA. Since no correctly-labeled ITCs were affected by the threshold, overall accuracy remained at 85.5%. However, the threshold helped decrease the commission error for BAEL and DIPA by 2.3% and 0.9%, respectively, and so the threshold appears useful for filtering ITCs with low accuracies.

3.5.2. Multispectral, broadband classification

Object-based LDA and ML classification accuracies were significantly greater for 10–30 narrowband, HYDICE imagery than for simulated IKONOS and ETM broadband imagery, which had 4 and 6 bands, respectively (Table 9). Overall accuracy with ASTER data (9 bands) and an ML classifier was 78.0% ($Pixel_{SUN}$), which was not significantly lower than the object-based accuracies achieved using 10–30 HYDICE bands with either the LDA or ML classifiers.

4. Discussion

4.1. Spatial scale and the spectral classification of TRF tree species

There was a decrease in classification accuracy from fine to coarser scales of spectral measurement (i.e., leaf to pixel and crown scales). Some of this trend can be explained by the differences in sensors used. Leaf-scale spectra had a relatively high ratio of signal to noise because they were measured in a controlled laboratory environment with a well-calibrated, high spectral resolution instrument. In contrast, pixel- and crown-scale spectra had considerably more noise due to poor sensor radiometric calibration and atmospheric effects.

Leaf spectral variability among individuals of a certain species, or even within a single crown, was attributed to differences in internal leaf structure and biochemistry (e.g., water, chlorophyll content, epiphyll cover and herbivory). Leaves have non-Lambertian properties and physical differences in adaxial leaf cuticle (e.g., micro-topography, wax, leaf hairs) affect first-surface specular reflectance, especially in the VIS region with large incident and/or view angles (Grant, 1987). Another source of variability among leaves of the same species was thus introduced by measuring laboratory bidirectional (as opposed to hemispherical) reflectance with varying leaf orientations.

Despite the multiple factors causing spectral variation, we found that leaf spectral variability among species was significantly greater than that within species. Cross-validation classifications confirmed that leaf-scale reflectance could discriminate among species with >89% overall accuracy using as few as 10 optimally-positioned bands. Important bands were concentrated in the NIR and SWIR1, where diffuse-reflectance dominates and variability is largely controlled by internal leaf structure and water content (Gausman, 1985; Grant, 1987).

Pixel-scale measurements acquired with the airborne hyperspectral sensor were dominated by leaf-scale spectral properties. Water absorption was enhanced at this coarser scale by multiple-scattering of photons among leaves, stems and branches (Asner, 1998; Roberts et al., 2004). In the NIR region, high levels of multiple-scattering caused the 980 and 1200 nm water absorption features to deepen, and overall NIR variability increased. The band-selection scheme for pixel spectra identified important bands bordering the NIR water absorption features, possibly detecting species differences in photon scattering caused by fine-scale crown architecture (e.g., LAI). Bands in the visible part of the spectrum were also important at pixel scales when considering all sunlit and shaded samples. The blue-green edge, yellow edge and red well bands chosen may be sensitive to species differences in spectral properties caused by their relative spectral mixing of leaf and bark fractions; however, our data do not allow us to test this hypothesis. We originally hypothesized that isolating sunlit regions of crowns for pixel-scale analysis would lower within-species spectral variance and enhance species separability. This hypothesis was confirmed by larger sunlit-sample F-ratios with spectral

angle and Euclidean distance metrics (Table 5). LDA and ML classifications also showed significant improvements in accuracy with $Pixel_{SUN}$ over $Pixel_{ALL}$ samples (Table 6). Gong et al. (1997) found similar results when classifying conifer spectra acquired at 6–8 cm spatial scales.

At the crown scale, the architectural arrangement of crown components, such as leaves and branches, controls the relative amounts of shading and complex, anisotropic multiple-scattering of photons relative to the illumination and view geometry described by each crown's bidirectional reflectance distribution function (BRDF). Crown-scale spectra in this study were a linear average of within-crown pixel spectra. The averaging of shadowed and bright pixels lowered mean crown-scale reflectance, and as is expected by averaging, crown-scale variance was low relative to pixel-scale variance. Band selection indicated that the NIR and SWIR2 were the main regions producing crown-scale separability among species. As with pixel-scale spectra, NIR reflectance is largely controlled by structural properties (e.g., density and arrangement of leaves) that influence the photon scattering environment and subsequent NIR reflectance. SWIR2 variability among species may be related to two factors: overall differences in crown water concentration that affects the expression of water absorption features at 1400, 1900 and 2700 nm (Gausman, 1985; Roberts et al., 2004); and, lignocellulose absorption features that may be expressed when high fractions of non-photosynthetic woody tissues are exposed to the sensor (Asner, 1998; Curran, 1989), such as in a low-LAI deciduous crown. Other methods for capitalizing on species-level differences caused by crown structure and their influence on high spatial resolution imagery are discussed in Section 4.2.

The SAM classifier was the least successful of the classifiers, regardless of the spatial scale or spectral region considered. This result was surprising since there were highly significant statistical separations of species with the spectral angle metric at leaf and pixel scales (Table 5). SAM does not use second-order statistics (e.g., covariance), and basing a classification on a single distance metric appears ineffective given within-species spectral diversity.

LDA was highly accurate at all scales of analysis, indicating that spectral covariance information—pooled for all species—is important for species discrimination. The leaf-scale and crown-scale ML classifiers may not have performed as well as LDA because of two factors. For one, the bands selected by the stepwise procedure were optimized for LDA classification. Other band-selection techniques, such as using Bhattacharyya distance (Haertel & Landgrebe, 1999), may improve ML classification accuracy. Furthermore, ML requires a large number of training samples for adequate estimation of the class covariance matrices from higher-dimensional data that may contain redundant and noisy information. Only with pixel-scale and object-based classifications did we have a large enough sample size to adequately assess ML with high dimensional data (i.e., 20+ bands). Although ML performed slightly better at pixel scales relative to LDA, object-based classifications were generally higher with LDA. The apparent advantage of the ML classifier at pixel scales may be spurious because only subsets of pixels from ITCs were used for training and testing in the analyses, while object-based classifications used all ITC pixels through cross-validation. The crown-scale ML classifications suffered from a lack of samples (individual trees) when estimating class covariance matrices. Collecting large training sets is challenging in TRF because target species have low densities, thus requiring large field surveys of forest that is often difficult to access. The LDA classifier appears more appropriate for TRF species discrimination because it strengthens the covariance estimation by pooling information from all species.

Results from our pixel-scale LDA classification analysis can be compared to a study by Fung et al. (1998), who used laboratory measurements of branch spectra to classify 12 subtropical tree species with 84% overall accuracy (Producer's accuracies from 56% to 100%). LDA and 90 bands from VIS to NIR were used in the analysis. In our analysis of sunlit pixels (i.e., branch scale) and 60 bands (VIS to SWIR2 sampled), our overall classification accuracy was 85% and Producer's accuracies ranged from 74% to 95%. Overall accuracy did not increase when using the full-spectrum of 161 bands. These results are encouraging since our airborne data suffers from multiple factors that could confound species discrimination, such as mixed pixels in training and testing data, variable illumination and viewing geometry, and noise introduced by atmospheric conditions and non-target biological organisms (e.g., lianas).

At all scales of observation, we noted an increase in accuracy with increased data dimensionality to a certain level. Results using the LDA and ML classifier revealed a general increase in accuracy up to 30 bands, while including more bands yielded equal or lower accuracy.

Our results confirm the benefits of hyperspectral over multispectral data for TRF tree identification. At all scales, the best accuracies with hyperspectral data were higher than those achieved with simulated multispectral imagery. Here we have applied fairly conventional analytical techniques that select optimal bands and then apply classifiers to narrowband reflectance values. Band selection was a necessary analytical step to isolate the most important bands for reliable classifier parameter estimation given our training data limitations (Duda & Hart, 1973). However, one major advantage of contiguous hyperspectral bands is their continuous description of spectral space, allowing measurements of the shape and position of key spectral features, such as liquid water absorption features in NIR. Purely hyperspectral analytical techniques exist and include spectral shape filters (Cochrane, 2000) and analyses of spectral first- and second-order derivatives. First-order derivatives have been shown to improve tree species classifications over the use of reflectance spectra (Gong et al., 1997; van Aardt & Wynne, 2001). However, current research has relied upon data from portable spectrometers in anticipation of high spatial and spectral

resolution data from future airborne or spaceborne sensors. Abiotic and biotic noise, such as atmospheric water vapor, epiphytes, and lianas, will complicate the radiance from a TRF canopy acquired by an airborne or satellite sensor, and much research is needed to test hyperspectral-based classification techniques under these challenging conditions.

4.2. Classification of individual tree crowns

Classifications of ITCs using crown-scale spectra had relatively high accuracies. The maximum accuracy achieved was 92% with the LDA classifier and 30 bands. Producer's accuracies ranged from 70% (CEPE) to 100% (TEOB), and User's accuracies ranged from 81% (LEAM) to 100% (TEOB). Our overall classification accuracy is higher than the 65% accuracy Leckie and Gougeon (1999) observed for temperate hardwood classification with crown-scale spectra, and it is similar to the 93% accuracy achieved by van Aardt and Wynne (2001) using in situ crown-scale spectra to classify 3 hardwood tree species (second derivatives used, sunlit samples). As reported in studies with conifer trees (Gougeon, 1995; Leckie et al., 2003), there was no evidence that sunlit crown spectra could be more accurately classified than by averaging the spectra from all pixels within the crown. Our results are encouraging considering that with visual interpretation of tropical tree species, Clément and Guellec (1974) could only identify their target species with 73% accuracy, and Myers and Benson (1981) visually-interpreted only 22% of their species with >75% accuracy. We therefore conclude that spectral-based classification of TRF tree species is possible, and accuracy is comparable or potentially greater than from visual interpretation of aerial photographs. Furthermore, computer-based classification permits the automation and removal of subjectivity from the process.

In the crown-scale LDA classification, there was inter-species confusion between individuals of *Lecythis* and *Dipteryx* (LEAM and DIPA, Table 7). This confusion is attributed to the deciduous phenology of these species–individuals had very low crown LAI and similar spectral properties. Bark lichen, epiphytes, and understory plants are also more likely to be exposed to the sensor in low-LAI crowns, and spectra from these components could dilute tree species spectral differences. Crown-scale spectra from DIPA and LEAM crowns were thus distinct from other species, but confused between the two species.

Despite this confusion, DIPA crowns had 92.6% Producer's accuracy and 89.3% User's accuracy (Table 7). Furthermore, the User's accuracy could be increased to 91.8% by applying a LDA probability threshold (Table 8). These results are encouraging because large *Dipteryx* trees have an important ecological function in providing a major seed resource and nesting cavities for the endangered Great green macaw (*Ara ambigua*) (pers. comm., Powell, 2001). Deforestation in the Sarapiquí region has mostly eliminated large *Dipteryx* trees outside of protected areas, thereby contributing to a dramatic decline in the macaw population. Remote sensing technology that can identify large *Dipteryx* crowns may contribute to macaw conservation efforts by providing a rapid and cost-effective means to map macaw habitat and migration corridors across the region.

In this study, another ITC classification technique was to label crown objects using the majority class of classified within-crown pixels. Relative to crown-scale LDA classification with 30 optimal bands, the object-based classification scheme had 8.5% and 2.4% lower accuracy with $Pixel_{ALL}$ and $Pixel_{SUN}$ samples, respectively (Table 6). However, one operational advantage of the object-based approach to ITC classification is that robust training statistics (e.g., the covariance matrix) can be estimated from a relatively small number of individual crowns per species because each crown contains many pixels. Furthermore, the object-based approach allows for the inevitable spectral variation within crowns that leads to misclassified samples. We observed that correctly-labeled ITCs had a mean within-crown pixel class accuracy of 90%. ITCs with more mixed-class pixels had more suspect species labels and were often mislabeled. We found that a pixel-majority threshold (e.g., majority class must have $\geq$35% of within-crown pixels) could be used to improve species User's accuracy by excluding low-accuracy ITCs and reducing commission errors; and, overall accuracy was left unchanged with the threshold. In contrast, crown-scale spectra blur within-crown variation. Basing an ITC species label on a single, crown-scale spectrum classification is risky due to relatively weak spectral separation among species (Table 5, Euclidean distance). This study benefited from distinct phenological differences among species, which undoubtedly helped crown-scale species discrimination. The object-based approach to classification may prove useful if ITCs are more spectrally confused due to similar phenology and crown architecture.

IKONOS and ETM+ overall accuracies were both lower than 67% for crown-scale and object-based ITC classifications. Since we used 1.6-m simulated multispectral data, none of our tests considered the actual resolution of existing sensors. The IKONOS multispectral sensor provides 4-m resolution images and so could be amenable to either a crown-scale or object-based classification scheme. However, we found that 1.6-m resolution pixels with IKONOS-simulated bands only provided 62% overall accuracy and DIPA User's accuracy was 64% (LDA, $Crown_{SUN}$). However, nine ASTER bands could classify ITCs with 77% overall accuracy with $Crown_{SUN}$ spectra, and DIPA User's accuracy was 76%. ASTER has 2 VIS, 1 NIR, 1 SWIR1 and 5 SWIR2 bands, while IKONOS contains only 3 VIS and 1 NIR bands. These additional SWIR2 bands in ASTER help discriminate species. This conclusion is supported by our hyperspectral, narrowband analyses, which also indicated that SWIR2 was important for species discrimination.

At crown scales, ten narrow bands from HYDICE imagery—with wavelength positions in all spectral

regions—produced 85% overall accuracy and DIPA User's accuracy was 93%. We therefore conclude that a high spatial resolution sensor with 10+ channels across the VIS to SWIR2 spectrum is necessary to classify TRF tree species with reasonable accuracy (i.e., ≥85%). For a satellite sensor, finer spectral resolution requires coarser fields of view due to limited surface photon flux. Likewise, airborne sensors can cover a larger swath if flown at a higher altitude with coarser spatial resolution pixels. Our crown-scale results indicate that a spatial resolution at the scale of tree crowns is adequate for species discrimination. However, our technique calculated crown-scale spectra by averaging only those spectra from within the ITC footprint, and in an operational situation, coarse-scale square pixels (e.g., 10–30 m) may subsume background plant species, soil and shadows, thereby producing mixed spectra and decreased classification accuracy. Future studies should thus examine the sensitivity of classification accuracy to spatial resolutions expected in operational circumstances (i.e., >1.6 m but less than the scale of a crown).

In our study, we analyzed emergent trees for two reasons: to be certain crowns could be identified in the imagery given georegistration errors, and to sample an adequate number of pixels per crown. Higher spatial resolution sensors will allow the investigation of more TRF tree species, especially co-dominant individuals that do not have broad, emergent crowns. Leaf-scale analyses indicated that spectral measurements with a very fine FOV are more accurately classified than spectrally-mixed pixels from coarser spatial scales. For example, leaf spectra were classified with 89% accuracy with just 10 bands and LDA classifier, while pixel and crown-scale accuracies were <85% for the same combination of bands and classifier (Table 6). However, these leaf-scale results are based on controlled laboratory conditions with a few species; spectra measured at this fine of scale from an airborne sensor will include atmospheric effects and spectral mixing from photon scattering among various crown tissues and other plant species. It is thus unclear if airborne digital sensors with very high resolutions (i.e., leaf scale) will allow species discrimination with relatively few bands (e.g., Meyer et al., 1996).

Given the dominant role of NIR for species separability at crown scales, we hypothesize that there exist species-level differences in crown structure that influence the volume-scattering properties of our tree species. Crown structure attributes, such as texture and foliage cover, are important for human-vision interpretation of TRF trees in aerial photographs (Trichon, 2001). In digital spectral imagery, crown structure will influence the spatial covariance structure of spectral vectors (i.e., pixels) in each crown, and the spectral-based analyses presented in our study do not include this spatial component. The use of spatial information for ITC species identification has not been fully explored in any forest environment. Meyer et al. (1996) found that classification of four tree species (3 conifers, 1 hardwood) in 0.16-m, 4-band multispectral data was 87% with a parallel-piped object-based approach that included texture (standard deviation of within-crown pixels in a 5 × 5 kernel), which was an improvement of 16% over using a ML classifier with 3 spectral bands and no texture. However, Leckie et al. (2003) later found that standard deviation texture did not improve conifer and hardwood species composition classification when considering the percent of individual species classified correctly at a stand scale. Much research is still needed to capture the spatial information content in high resolution imagery for TRF species discrimination.

4.3. Potential for tropical rain forest natural resource management

This study has demonstrated the potential of high spatial and spectral resolution imagery for the species-level or floristic classification of tropical rainforest trees. Results are preliminary in that our crown-scale and object-based approaches were limited to 1) 1.6-m spatial resolution imagery, 2) conventional spectral classification techniques that do not fully exploit the spectral or spatial detail of the imagery, 3) only canopy-emergent individuals of 7 out of 400+ tree species in our study site, and 4) manually-digitized crowns. In future research, we will explore purely hyperspectral-based analytical techniques for species classification, such as multiple-endmember spectral mixture analysis (Roberts, Gardner et al., 1998) and absorption feature analysis (Kokaly & Clark, 1999), as well as incorporation of spatial information related to crown structure. Operational applications involving individual tree inventory over large spatial extents will require automated methods of isolating crowns in the imagery. Automated ITC delineation is a subdiscipline of image segmentation and is an area of intense research (reviewed extensively in McGraw et al., 1998 and Key et al., 2001). Most segmentation methods have been developed for forestry applications in conifer-dominated stands and there are still many challenges to crown delineation in complex, old-growth hardwood forests, where trees and lianas may intertwine and overlap, inter-tree shadows are narrow, and canopy-gap shadows are prevalent, causing automated segmentation schemes to identify clusters of trees rather than individual crowns (McGraw et al., 1998).

As publicly-available sensors improve in spatial and spectral detail, ITC species identification in TRF could be an operational reality. Applications include the location and monitoring of commercially-valuable species such as mahogany, assessment of habitat in reserves, fragments and biological corridors, analyses of biodiversity patterns relative to environmental factors, and monitoring of demographic changes in tree communities due to global warming.

Phenology is an important consideration in mapping TRF tree species. In this study, deciduous *Dipteryx* and *Lecythis* trees in near leaf-off conditions had distinct volume-scattering and spectral mixing properties relative to other species. It is unclear from our results whether band selection and classification accuracies would have changed if the imagery

had been flown in the wet season, when *Dipteryx* and *Lecythis* have crowns fully-flushed with leaves. Also, phenological events such as senescence before leaf drop or flowering produce changes in reflectance spectra that may be amplified in leaf-on conditions due to volumetric scattering. If these changes in spectral reflectance occur synchronously in all individuals of the target population and do not overlap in time with other species, then image acquisition may be timed to maximize classification accuracy for a particular target species. For example, *Dipteryx* has pink flowers and is known to flower with a peak between May and August when trees have leaves (Frankie et al., 1974; Newstrom et al., 1994; O'Brien, 2001). However, TRF tree phenology is complex, little understood, and difficult to generalize; at LSBS, *Ceiba* (CEPE) flower in the dry season when trees are leafless, *Terminalia* (TEOB) populations have variation in annual flowering intensity, and some overstory trees in the LSBS forest have asynchronous flowering among individuals of the same species (Frankie et al., 1974).

5. Conclusions

Our results confirm that species of tropical rain forest (TRF) trees can be discriminated based on their spectral reflectance properties. Individual tree crowns (ITCs) were successfully classified with 92% overall accuracy using 30 optimally-selected bands from crown-scale reflectance spectra and a linear discriminant analysis classifier. Object-based ITC classification, which labeled crowns based on within-crown classified pixels, was not as accurate as crown-scale spectra classification. At a fixed 1.6-m spatial scale, crown-scale ITC classification was significantly more accurate with hyperspectral narrowband data (10 band HYDICE) relative to accuracies achieved with multispectral broadband data (simulated IKONOS, Landsat ETM+ and ASTER).

This study represents the first use of high spectral and spatial resolution imagery acquired over TRF canopy for automated discrimination of individual tree species. Similar to laboratory-based analyses by Cochrane (2000), our results indicate that there are spectral differences among species that permit classification at leaf to crown scales; however, there is also temporal and spatial spectral variation within populations and even single individuals of TRF tree species that will inevitably decrease classification accuracy. A major challenge is to develop classification schemes that can maximize the spectral, spatial and temporal information content of digital imagery while accommodating inherent variation within species.

Acknowledgements

This work was supported by NASA Headquarters under the Earth System Science Fellowship Grant NGT5-30436. NASA's AVIRIS team at the Jet Propulsion Laboratory provided the ASD field spectrometer used for measuring laboratory and field spectra. Old-growth tree data used in this study were from research supported by the National Science Foundation under Grant DEB-0129038 and the Andrew W. Mellon Foundation. HYDICE data were donated to OTS by the U.S. Naval Research Laboratory. OTS provided logistical support for the hyperspectral data acquisition. The authors would like to thank Leonel Campos and William Miranda for field assistance and fine marksmanship in collecting leaf samples, as well as Dr. Stephanie Bohlman, Seth Peterson and five anonymous reviewers for helping to improve this manuscript.

References

Achard, F., Eva, H. D., Stibig, H. J., Mayaux, P., Gallego, J., Richards, T., et al. (2002). Determination of deforestation rates of the world's humid tropical forests. *Science*, *297*(5583), 999–1002.

Anderson, M. J. (2001). A new method for non-parametric multivariate analysis of variance. *Austral Ecology*, *26*(1), 32–46.

Anderson, M. J. (2004). *DISTLM v.5: A FORTRAN computer program to calculate a distance-based multivariate analysis for a linear model*. New Zealand: Department of Statistics, University of Auckland.

Asner, G. P. (1998). Biophysical and biochemical sources of variability in canopy reflectance. *Remote Sensing of Environment*, *64*(3), 234–253.

Basedow, R. W., Carmer, D. C., & Anderson, M. E. (1995). HYDICE system: Implementation and performance. *SPIE Proceedings*, *Vol. 2480*, Feb. 17–24, Orlando, FL, USA.

Castro-Esau, K. L., Sánchez-Azofeifa, G. A., & Caelli, T. (2004). Discrimination of lianas and trees with leaf-level hyperspectral data. *Remote Sensing of Environment*, *90*, 353–372.

Clark, D. A., Piper, S. C., Keeling, C. D., & Clark, D. B. (2003). Tropical rain forest tree growth and atmospheric carbon dynamics linked to interannual temperature variation during 1984–2000. *Proceedings of the National Academy of Sciences of the United States of America*, *100*(10), 5852–5857.

Clark, D. B., Clark, D. A., & Read, J. M. (1998). Edaphic variation and the mesoscale distribution of tree species in a neotropical rain forest. *Journal of Ecology*, *86*(1), 101–112.

Clark, D. B., Read, J. M., Clark, M. L., Murillo Cruz, A., Fallas Dotti, M., & Clark, D. A. (2004a). Application of 1-m and 4-m resolution satellite data to studies of tree demography, stand structure and land-use classification in tropical rain forest landscapes. *Ecological Applications*, *14*(1), 61–74.

Clark, M. L., Clark, D. B., & Roberts, D. A. (2004b). Small-footprint lidar estimation of sub-canopy elevation and tree height in a tropical rain forest landscape. *Remote Sensing of Environment*, *9*(1), 68–89.

Clément, J., & Guellec, J. (1974). Utilization des photographies aériennes au 1/5.000 en coleur pour la détection de l'Okoumé dans la forêt dense du Gabon. *Bois et Forêts des Tropiques*, *153*, 3–22.

Cochrane, M. A. (2000). Using vegetation reflectance variability for species level classification of hyperspectral data. *International Journal of Remote Sensing*, *21*(10), 2075–2087.

Cochrane, M. A., Alencar, A., Schulze, M. D., Souza, C. M., Nepstad, D. C., Lefebvre, P., et al. (1999). Positive feedbacks in the fire dynamic of closed canopy tropical forests. *Science*, *284*(5421), 1832–1835.

Congalton, R. G., & Mead, R. A. (1983). A quantitative method to test for consistency and correctness in photointerpretation. *Photogrammetric Engineering and Remote Sensing*, *49*(1), 69–74.

Curran, P. J. (1989). Remote sensing of foliar chemistry. *Remote Sensing of Environment*, *30*(3), 271–278.

Dixon, R. K., Brown, S., Houghton, R. A., Solomon, A. M., Trexler, M. C., & Wisniewski, J. (1994). Carbon pools and flux of global forest ecosystems. *Science*, *262*, 185–190.

Duda, R. O., & Hart, P. E. (1973). *Pattern classification and scene analysis*. New York: John Wiley and Sons, Inc.

Fearnside, P. M. (1999). Biodiversity as an environmental service in Brazil's Amazonian forests: risks, value and conservation. *Environmental Conservation*, *26*(4), 305–321.

Foody, G. M. (2003). Remote sensing of tropical forest environments: Towards the monitoring of environmental resources for sustainable development. *International Journal of Remote Sensing*, *24*(20), 4035–4046.

Foody, G. M., Boyd, D. S., & Cutler, M. E. J. (2003). Predictive relations of tropical forest biomass from Landsat TM data and their transferability between regions. *Remote Sensing of Environment*, *85*(4), 463–474.

Frankie, G. W., Baker, H. G., & Opler, P. A. (1974). Comparative phenological studies of trees in tropical wet and dry forests in the lowlands of Costa Rica. *Journal of Ecology*, *62*(3), 881–919.

Fung, T., Ma, F. Y., & Siu, W. L. (1998). Hyperspectral data analysis for subtropical tree species recognition. *Symposium proceedings, IGARSS '98, sensing and managing the environment*, *vol. 3* (pp. 1298–1300). New York, NY, USA: IEEE International Geoscience and Remote Sensing, Seattle, WA, USA, July 6–10, 1998.

Gao, B. C., & Goetz, A. F. H. (1990). Column atmospheric water-vapor and vegetation liquid water retrievals from airborne imaging spectrometer data. *Journal of Geophysical Research, D: Atmospheres*, *95*, 3549–3564.

Gausman, H. W. (1985). *Plant leaf optical properties in visible and near-infrared light*. Lubbock, Texas: Texas Tech Press.

Gillespie, T. W., Brock, J., & Wright, C. W. (2004). Prospects for quantifying structure, floristic composition and species richness of tropical forests. *International Journal of Remote Sensing*, *25*(4), 707–715.

Gong, P., Pu, R. L., & Yu, B. (1997). Conifer species recognition: An exploratory analysis of in situ hyperspectral data. *Remote Sensing of Environment*, *62*(2), 189–200.

Gougeon, F. A. (1995). Comparison of possible multispectral classification schemes for tree crowns individually delineated on high spatial resolution MEIS images. *Canadian Journal of Remote Sensing*, *21*, 1–9.

Gougeon, F. A., & Leckie, D. G. (2003). Forest information extraction from high spatial resolution images using an individual tree crown approach. *Information Report BC-X-396*. Victoria, British Columbia, Canada: Pacific Forestry Centre, Canadian Forest Service.

Grant, L. (1987). Diffuse and specular characteristics of leaf reflectance. *Remote Sensing of Environment*, *22*, 309–322.

Haertel, V., & Landgrebe, D. A. (1999). On the classification of classes with nearly equal spectral response in remote sensing hyperspectral image data. *IEEE Transactions on Geoscience and Remote Sensing*, *37*(5), 2374–2386.

Hartshorn, G. S., & Hammel, B. E. (1994). Vegetation types and floristic patterns. In L. A. McDade, K. S. Bawa, H. A. Hespenheide, & G. S. Hartshorn (Eds.), *La Selva: Ecology and natural history of a neotropical rain forest* (pp. 73–89). Chicago: University of Chicago Press.

Herwitz, S. R., Slye, R. E., & Turton, S. M. (1998). Redefining the ecological niche of a tropical rain forest canopy tree species using airborne imagery: Long-term crown dynamics of *Toona ciliata*. *Journal of Tropical Ecology*, *14*, 683–703.

Hudson, W. D., & Ramm, C. W. (1987). Correct formulation of the kappa coefficient of agreement. *Photogrammetric Engineering and Remote Sensing*, *53*(4), 421–422.

Jackson, Q., & Landgrebe, D. A. (2001). An adaptive classifier design for high-dimensional data analysis with a limited training data set. *IEEE Transactions on Geoscience and Remote Sensing*, *39*(12), 2664–2679.

Key, T., Warner, T. A., McGraw, J. B., & Fajvan, M. A. (2001). A comparison of multispectral and multitemporal information in high spatial resolution imagery for classification of individual tree species in a temperate hardwood forest. *Remote Sensing of Environment*, *75*(1), 100–112.

Kokaly, R. F., & Clark, R. N. (1999). Spectroscopic determination of leaf biochemistry using band-depth analysis of absorption features and stepwise multiple linear regression. *Remote Sensing of Environment*, *67*(3), 267–287.

Kruse, F. A., Lefkoff, A. B., Boardman, J. W., Heidebrecht, K. B., Shapiro, A. T., Barloon, P. J., et al. (1993). The spectral image-processing system (SIPS)-interactive visualization and analysis of imaging spectrometer data. *Remote Sensing of Environment*, *44*(2-3), 145–163.

Krzanowski, W. J. (2001). Data-based interval estimation of classification error. *Journal of Applied Statistics*, *28*(5), 585–595.

Laurance, W. F., Oliveira, A. A., Laurance, S. G., Condit, R., Nascimento, H. E. M., Sanchez-Thorin, A. C., et al. (2004). Pervasive alteration of tree communities in undisturbed Amazonian forests. *Nature*, *438*, 171–175.

Leckie, D. G., & Gougeon, F. A. (1999). An assessment of both visual and automated tree counting and species identification with high spatial resolution multispectral imagery. *Proceedings of the international forum: Automated interpretation of high spatial resolution digital imagery for forestry.* Victoria, British Columbia, February 10–12, 1998 (pp. 141–154). Victoria, BC: Canadian Forest Service, Pacific Forestry Centre.

Leckie, D. G., Gougeon, F. A., Walsworth, N., & Paradine, D. (2003). Stand delineation and composition estimation using semi-automated individual tree crown analysis. *Remote Sensing of Environment*, *85*(3), 355–369.

McArdle, B. H., & Anderson, M. J. (2001). Fitting multivariate models to community data: A comment on distance-based redundancy analysis. *Ecology*, *82*(1), 290–297.

McGraw, J. B., Warner, T. A., Key, T. L., & Lamar, W. R. (1998). High spatial resolution remote sensing of forest trees. *Trends in Ecology and Evolution*, *13*(8), 300–301.

Meyer, P., Staenz, K., & Itten, K. I. (1996). Semi-automated procedures for tree species identification in high spatial resolution data from digitized colour infrared-aerial photography. *ISPRS Journal of Photogrammetry and Remote Sensing*, *51*(1), 5–16.

Myers, B. J., & Benson, M. L. (1981). Rainforest species on large-scale colour photos. *Photogrammetric Engineering and Remote Sensing*, *47*, 505–513.

Nagendra, H. (2001). Using remote sensing to assess biodiversity. *International Journal of Remote Sensing*, *22*(12), 2377–2400.

Newstrom, L. E., Frankie, G. W., Baker, H. G., & Colwell, R. K. (1994). Diversity of long-term flowering patterns. In L. A. McDade, K. S. Bawa, H. A. Hespenheide, & G. S. Hartshorn (Eds.), *La Selva: Ecology and natural history of a neotropical rain forest* (pp. 142–160). Chicago: University of Chicago Press.

O'Brien, J. J. (2001). *The effects of climate on the growth and physiology of tropical rainforest trees.* PhD Dissertation. Florida International University, Miami, Florida.

Poorter, L., Oberbauer, S. F., & Clark, D. B. (1995). Leaf optical-properties along a vertical gradient in a tropical rain-forest canopy in Costa-Rica. *American Journal of Botany*, *82*(10), 1257–1263.

Powell, G. (2001). Senior Conservation Scientist, World Wildlife Fund, Monteverde, Costa Rica. Personal communication.

Powell, R. L., Matzke, N., de Souza Jr., C., Clark, M., Numata, I., Hess, L. L., et al. (2004). Sources of error in accuracy assessment of thematic land-cover maps in the Brazilian Amazon. *Remote Sensing of Environment*, *90*, 221–234.

R Development Core Team. (2004). *R: A language and environment for statistical computing*. Vienna, Austria: R Foundation for Statistical Computing, ISBN: 3-900051-07-0 http://www.R-project.org

Read, J. M., Clark, D. B., Venticinque, E. M., & Moreira, M. P. (2003). Application of merged 1-m and 4-m resolution satellite data to research and management in tropical forests. *Journal of Applied Ecology*, *20*, 592–600.

Roberts, D. A., Gardner, M., Church, R., Ustin, S., Scheer, G., & Green, R. O. (1998). Mapping chaparral in the Santa Monica Mountains using multiple endmember spectral mixture models. *Remote Sensing of Environment*, *65*(3), 267–279.

Roberts, D. A., Nelson, B. W., Adams, J. B., & Palmer, F. (1998). Spectral changes with leaf aging in Amazon caatinga. *Trees-Structure and Function*, *12*(6), 315–325.

Roberts, D. A., Numata, I., Holmes, K., Batista, G., Krug, T., Moteiro, A., et al. (2002). Large area mapping of land-cover change in Rondônia using multitemporal spectral mixture analysis and decision tree classifiers. *Journal of Geophysical Research, D: Atmospheres*, *107*(20), 8073.

Roberts, D. A., Ustin, S. L., Ogunjemiyo, S., Greenberg, J., Dobrowski, S. Z., Chen, J., et al. (2004). Spectral and structural measures of Northwest forest vegetation at leaf to landscape scales. *Ecosystems*, *7*(5), 545–562.

Rocchio, L.E. (2000). *Lidar remote sensing of sub-canopy topography.* Master's Thesis, University of Maryland, College Park, Maryland, USA.

Skole, D., & Tucker, C. (1993). Tropical deforestation and habitat fragmentation in the Amazon—satellite data from 1978 to 1988. *Science*, *260*(5116), 1905–1910.

Steininger, M. K., Tucker, C. J., Townshend, J. R. G., Killeen, T. J., Desch, A., Bell, V., et al. (2001). Tropical deforestation in the Bolivian Amazon. *Environmental Conservation*, *28*(2), 127–134.

Tabachnick, B. G., & Fidell, L. S. (1989). *Using multivariate statistics*, (Second Edition). New York, USA: Harper Collins Publishers, Inc.

Thomas, C. D., Cameron, A., Green, R. E., Bakkenes, M., Beaumont, L. J., & Collingham, Y. C. (2004). Extinction risk from climate change. *Nature*, *427*(6970), 145–148.

Trichon, V. (2001). Crown typology and identification of rain forest trees on large-scale aerial photographs. *Plant Ecology*, *153*, 301–312.

Tuomisto, H., Poulsen, A. D., Ruokolainen, K., Moran, R. C., Quintana, C., Celi, J., et al. (2003). Linking floristic patterns with soil heterogeneity and satellite imagery in Ecuadorian Amazonia. *Ecological Applications*, *13*(2), 352–371.

van Aardt, J. A. N., & Wynne, R. H. (2001). Spectral separability among six southern tree species. *Photogrammetric Engineering and Remote Sensing*, *67*(12), 1367–1375.

Whitmore, T. C. (1990). *An introduction to tropical rain forests*. Oxford: Clarendon Press.

Woolley, J. T. (1971). Reflectance and transmittance of light by leaves. *Plant Physiology*, *47*, 656–662.